1 **Technical Reviews**

2 **Optical vegetation indices for monitoring terrestrial ecosystems globally**

3

4 Yelu Zeng [a], Dalei Hao [b], Alfredo Huete [c], Benjamin Dechant [d], Joe Berry [e], Jingming Chen [f],

5 Joanna Joiner [g], Christian Frankenberg [h,m], Ben Bond-Lamberty [i], Youngryel Ryu [j], Jingfeng Xiao [k],

6 Ghassem R. Asrar [l], Min Chen [a]

7

8 [a] Department of Forest and Wildlife Ecology, University of Wisconsin-Madison, 1630 Linden

9 Drive, Madison, WI, USA

10 [b] Atmospheric Sciences and Global Change Division, Pacific Northwest National Laboratory,

11 Richland, WA, USA

12 [c] School of Life Sciences, University of Technology Sydney, Sydney, NSW, Australia

13 [d] Synthesis Centre for Biodiversity Sciences, German Centre for Integrative Biodiversity Research,

14 Puschstraße 4, 04103 Leipzig, Germany

15 [e] Department of Global Ecology, Carnegie Institution for Science, Stanford, CA 94305, USA

16 [f] Department of Geography and Program in Planning, University of Toronto, Toronto, ON M5S

17 3G3, Canada

18 [g] NASA Goddard Space Flight Center, Greenbelt, MD, USA

19 [h] Division of Geological and Planetary Sciences, California Institute of Technology, Pasadena, CA,

20 USA

21 [i] Joint Global Change Research Institute, Pacific Northwest National Laboratory, College Park,

22 MD 20740, USA

23 [j] Department of Landscape Architecture and Rural Systems Engineering, Seoul National University,

24 South Korea

25 [k] Earth Systems Research Center, Institute for the Study of Earth, Oceans, and Space, University of

26 New Hampshire, Durham, NH 03824, USA

27 [l] Universities Space Research Association, Columbia, MD 21046, USA

28   m Jet Propulsion Laboratory, California Institute of Technology, Pasadena, USA

29   Corresponding authors: Min Chen (mchen392@wisc.edu) and Dalei Hao (dalei.hao@pnnl.gov)

30

31   **Key points**

32   - Optical vegetation indices (VIs) derived from space-borne Earth observations are widely

33   used for monitoring terrestrial ecosystems including plant biophysical, biochemical and

34   physiological properties, vegetation dynamics and environmental stresses.

35   - Sensor and calibration effects, quality assurance and quality control (QA/QC) flags,

36   bidirectional reflectance distribution function (BRDF), atmospheric and topographic

37   effects, and snow/soil background are among important sources of VI-based uncertainties.

38   - Potential artefacts must be carefully considered to avoid biased interpretations of the

39   underlying ecological processes resulting from the improper use of VIs.

40   - VIs based on ratios of reflectance such as NDVI can help reduce sensor calibration, BRDF,

41   atmospheric and topographic effects, but could be sensitive to snow/soil background and

42   scale effects.

43   - NIRv has the biophysical meaning of FPAR times the photon escape ratio (*fesc*), and is

44   linearly correlated with EVI, EVI2 and DVI on a mathematical-basis, while ratio-based

45   NDVI behaves differently.

46   - Next generation VIs with greater signal sensitivity and less artefacts, are expected with

47   new hyperspectral/geostationary satellite missions and synergistic integration with other

48   metrics, providing advanced opportunities for studying terrestrial ecosystems.

49

Abstract

Vegetation indices (VIs) are widely used in studying vegetation dynamics across spatial (local, regional, and global) and temporal (sub-hourly, daily, seasonal, annual, and decadal) scales. However, diverging conclusions have often been reached for the same canopy conditions using different VIs, rendering past and present scientific studies by the ecological community ambiguous. In this review, we summarize the rationale, history and ecological applications of VIs, and provide useful insights on VI inconsistencies due to improper considerations of a variety of factors, such as the use of different VIs, sensors, satellite product versions, atmospheric and sun-target-sensor geometry corrections, compositing algorithms, and use of quality assurance and control (QA/QC) flags. The debate on Amazon forest greening in the dry season is used as an example to illustrate VI inconsistencies. We demonstrate that the photon escape ratio (*fesc*) from the canopy provides the mathematical- and physical-basis for the intrinsic linkage among several of the most widely used VIs. NIRv, EVI, EVI2 and DVI are strongly linearly correlated with each other while NDVI behaviors differently. Identifying key sensitive wavelengths for target application is the first step towards the optimal use of VIs, followed by an understanding of potential signal contamination sources in the specific ecosystem.

1. Introduction

Vegetation indices ('VIs') are simple mathematical combinations or transformations of reflectance in two or more spectral channels to represent vegetation status conditions (Fig. 1), while minimizing the impacts of other contributing factors such as the soil background, atmosphere and sun-target-sensor geometry[1-3]. As useful and efficient tools, VIs have attracted a large community of users from a wide range of scientific disciplines over the last half century. VIs are also easily obtained at different scales, from the ground with hand-held spectral sensing devices, tower-based and airborne sensors up to satellites, and hence can provide measurements from the fine to coarse resolutions. VIs are highly objective, with no or only minimal assumptions with regard to land cover type and canopy structure. As a result, they have been intensively used in local to global scale studies, and in almost every discipline of Earth science, especially in ecological research[4-6].

A number of VIs have been developed since the early 1970s (Table 1). Many of them can be easily calculated from publicly available remote sensing data, while the subtleties in processing and interpretation of results require more experience and theoretical background. With their wide adoption, VIs are increasingly applied to more challenging research questions/experiments to shed light on complex ecological topics such as vegetation response to long-term climate change[7-9], short-term disturbances[10,11] and extreme climate events[12]. The simplicity of VIs, however, can be deceptive as there are many cases of confusion, misinterpretations, and scientific controversies related to their use.

This review aims to inform scientists with the rationale, history, and key features of VIs that hopefully can be helpful for better understanding and using VIs for ecological studies. Although hundreds of VIs have been proposed, there is no necessity to go through all these VIs because many of them were built with similar formulae or principles. Instead, we will reinvestigate a selected subset of the most widely used VIs in this review, with a particular emphasis on clarifying and summarizing their usefulness, relationships, inconsistencies, artefacts and limitations. We also attempt to present recommendations on how to avoid these potential pitfalls to improve their use

94   for the wider ecological community. In addition, since most existing VIs are based on reflectance

95   in the optical wavelengths, we mainly focus on the optical VIs in this review, and particularly on

96   those having the potential to be derived by satellite observations and applied globally. We use a

97   few 'milestone' VIs as representative examples across our technical analyses, such as the

98   Normalized Difference Vegetation Index (NDVI), the Enhanced Vegetation Index (EVI), and the

99   Near-Infrared Reflectance of Vegetation (NIRv), which are among the most widely used VIs in a

100   variety of global-scale ecological studies and can reveal some common features of many VIs.

101   **2. Rationale of VIs**

102   The launch of Earth observing satellites since 1972 ushered a new era for global observation

103   and study of vegetation (Fig. 2)[13]. The physical foundation of VIs, as a product of the remotely-

104   sensed spectral reflectance, is built on our understanding of the complex light-vegetation

105   interactions. Essentially, satellite-measured spectral reflectance is a mixed signal of vegetation

106   canopies, their shadows, soils and possibly other components standing on the land surface, and is

107   commonly co-determined by leaf reflectance, the background soil reflectance, canopy structure,

108   and the sun-sensor geometry. The spectral signature of leaf reflectance is well understood (Fig. 1).

109   Leaf reflectance is relatively lower in the visible (VIS) domain (400~700 nm) because of the strong

110   absorption of photosynthetic pigments, particularly in the non-green wavelengths due to the

111   absorption of chlorophylls; high leaf reflectance in the near infrared band (NIR; 700~1300 nm) is

112   usually expected due to spongy mesophyll, and lower leaf reflectance happens in the shortwave

113   infrared (SWIR; 1300~2500 nm) due to strong water absorption and, to a less degree, other leaf

114   biochemical traits such as lignin, protein and cellulose content. A typical soil reflectance spectrum

115   monotonically increases with wavelength in the optical domain except the water absorptions in the

116   SWIR band. Canopy structure is a key factor for the canopy reflectance, because it determines how

117   much of the incoming light is reabsorbed, re-scattered and finally escapes from the canopies.

118   Biophysical or structural parameters such as Leaf Area Index (LAI), Leaf Angle Distribution (LAD)

119   and Clumping Index (CI) are commonly used to characterize canopy structure. The sun-sensor

120   geometry further complicates the canopy reflectance observations, largely due to the fraction of

121   shadows in view because of the varying relative positions of the light source (sun) and the sensor.

122   Furthermore, the atmospheric radiative transfer process is another important factor to consider in

123   practice.

124   Therefore, VIs have been developed based on the simple rationale that the spectral signals

125   from the vegetation, and more specifically, the vegetation characteristics of interest (for example,

126   vegetation biophysical, biochemical and physiological properties) should be enhanced with

127   properly designed mathematical combinations such as ratios, differences, derivative, or the

128   combinations of the ratios and differences between reflectance from different spectral wavelengths

129   or bands (Fig. 3). This enhancement goes along with reducing, or ideally suppressing background

130   signals from soil and confounding factors related to vegetation characteristics with overlapping

131   spectral features. However, even for a given vegetation characteristic, it is not straightforward to

132   use one single formula that holds under different conditions. This, together with the interest in

133   various different vegetation characteristics as well as increasing availability of more and more and

134   increasingly narrow spectral bands from satellite sensors, is driving the continuing development of

135   VIs.

136   **3. A Brief History of VIs**

137   *3.1 VIs for plant biophysical properties*

138   The history of VI developments goes back to the early 1970s (Fig. 2). The first-generation red-

139   NIR ratio- and difference-based VIs, including the Simple ratio (SR), Difference Vegetation Index

140   (DVI) and NDVI[14-16] were proposed to quantify vegetation growing condition based on the fact

141   that live green vegetation significantly absorbs solar radiation in red but reflects most of the solar

142   energy in NIR to support photosynthesis while avoiding potential damage from overheating[17] (Fig.

143   1). Further refinements have been introduced to minimize the effects of intervening soil

144   background and atmosphere to better isolate the vegetation contributions, especially for sparse

145   vegetation cover[1,18]. Examples include an orthogonal-transformation based perpendicular

146 vegetation index (PVI)[19], the soil adjusted vegetation index (SAVI)[3], Transformed SAVI

147 (TSAVI)[20] and Modified SAVI (MSAVI)[21]. Later, Modified Simple Ratio (MSR)[22] was formulated

148 based on the evaluation of several two-band VIs (for example, SR, NDVI and SAVI) for the

149 purpose of improving the linear relationship with biophysical parameters and reducing the

150 sensitivity to measurement noise[22]. Reduced SR (RSR) further increased the sensitivity and

151 correlation to LAI than SR, and reduced the effect of background reflectance by taking the canopy

152 closure and understory contribution of open canopies into account with the SWIR band included[23].

153   The Global Environment Monitoring Index (GEMI) was introduced to reduce the atmospheric

154 effects[24]. The launch of MODIS onboard NASA's Terra and Aqua satellites in the early 2000s

155 opened new opportunities for VI developments with more spectral bands in the optical wavelengths.

156 The Atmospherically Resistant Vegetation Index (ARVI) and EVI[25] were proposed to minimize the

157 atmospheric effects with an expected blue to red band 'atmosphere scatter' signal, enabling

158 correction from the blue and red band relative proportions[25,26]. As atmospheric correction

159 algorithms improved, the two-band version of EVI (EVI2)[27] with the absence of the blue-band was

160 developed in 2008 without blue band while achieving similar performance as compared with EVI[27].

161 In 2014, plant phenology index (PPI)[28] was derived for estimating plant canopy growth, especially

162 for evergreen forest phenology over high latitudes[28]. PPI has a nearly linear relationship with green

163 LAI, and soil brightness variations have moderate impact on PPI. More recently, NIRv[4] and the

164 fluorescence correction vegetation index (FCVI)[29] were added to the list because of their ability to

165 reduce soil background effects on the NIR reflectance of vegetation and to better approximate the

166 vegetation's solar radiation absorption and photosynthesis[4,30]. NIRv has received significant

167 attention and application because of its clear physical foundation and strong correlation with

168 vegetation photosynthesis (Fig. 3)[4,30]. In 2021, the kernel NDVI (kNDVI) was proposed based on

169 the theory of kernel methods as a unifying VI for monitoring the terrestrial carbon dynamics and

170 increasing the sensitivity of NDVI to plant biophysical parameters[31].

171 ***3.2 VIs for plant biochemical properties.***

172   Broad-band reflectance smooths the detailed spectral signatures and thus above-mentioned

173   broad-band VIs are primarily designed for detecting vegetation structure and its changes. In

174   parallel, a group of VIs were developed by taking advantage of narrow-band sensor measurements

175   that keep more detailed spectral information. In general, narrow-band VIs are specifically designed

176   to indicate the biochemical and physiological properties such as pigments, water, plant residues

177   and nitrogen[32], and typically use a combination of strong-absorbing VIS bands and a narrow band

178   located in the red-edge region (670~780nm). Examples include Red Edge Chlorophyll Index

179   (CIred-edge)[33], Red-edge NDVI (NDVIre)[34] and MERIS Total Chlorophyll Index (MTCI)[35] for

180   indicating chlorophyll content, the Structure Insensitive Pigment Index (SIPI)[36], Normalized

181   Pigments Chlorophyll Ratio Index (NPCI)[37], Plant Senescence Reflectance Index (PSRI)[38] for

182   carotenoid content, and Anthocyanin Reflectance Index (ARI)[39], Anthocyanin Content Index

183   (ACI)[40] and Red/Green Ratio Index (RGRI)[41] for anthocyanin content. Using the water absorption

184   bands around 970, 1200, 1450, 1940 and 2500 nm, Normalized Difference Water Index (NDWI)[42],

185   Land Surface Water Index (LSWI)[43,44], and Normalized Difference Infrared Index (NDII)[45] were

186   designed with a similar formula and exhibit similarly robust performance on indicating vegetation

187   hydrological condition[46]. The Normalized Difference Lignin Index (NDLI) was designed with the

188   1754 nm lignin absorption feature, and the Normalized Difference Nitrogen Index (NDNI)

189   considered the 1510 nm nitrogen absorption feature[47].

190   *3.3 VIs for plant physiological properties*

191   Another group of VIs were proposed to detect stress-induced physiological changes in

192   xanthophyll cycle pigments, as indicators of photosynthetic light use efficiency or environmental

193   stresses[48]. Because the reflectance at 531 nm is sensitive to carotenoid pigments and the

194   xanthophyll cycle, the Photochemical Reflectance Index (PRI) was proposed (with a reference

195   wavelength at 570 nm) in 1992 to track changes in diurnal photosynthetic efficiency[49]. The

196   Chlorophyll/Carotenoid Index (CCI) proposed in 2016 is another index for representing the

197   dynamics of the chlorophyll/carotenoid ratio and has the potential to track seasonal variations of

198   canopy photosynthesis at the global scale[5], because it could be directly obtained from existing

199   satellite data. PRI, CCI and green chromatic coordinate (GCC) can capture the seasonal variation

200   of carotenoid and xanthophyll cycles over temperate evergreen needleleaf forests that are difficult

201   to detect with broadband VIs such as NDVI and NIRv[50,51]. Red-edge Vegetation Stress Index

202   (RVSI)[52] had less negative values for stressed leaves than healthy leaves in grapevine leafroll

203   disease detection over two wine grape cultivars[53].

204   *3.4 Satellite sensors for VIs*

205   VIs can be calculated from reflectance measurements by a series of Earth-observing satellite

206   sensors[13] (Fig. 2). Landsat 1~3 MultiSpectral Scanner (MSS) since 1972 only had four VIS-NIR

207   bands with about 80-m spatial resolution and half-monthly revisit cycle, while since Landsat 4 was

208   launched in 1982, the spatial resolution in VIS-NIR bands has increased to 30-m. Sensors with

209   similar spatial resolution include SPOT (1986~) and Sentinel-2 (2015~), which have weekly to

210   daily temporal resolution. Sentinel-2 is one of the few sensors with the capability to calculate red-

211   edge VIs for plant pigments. AVHRR, MODIS and VIIRS, launched in 1981, 1999 and 2011,

212   respectively, have the daily temporal coverage, while AVHRR does not have the blue band for EVI.

213   Towards high temporal resolution, geostationary satellites, such as GOES and Himawari both

214   launched in the 1970s, had sub-hourly VI observations. NDVI, SR and RSR have been employed

215   to generate global LAI products from Himawari, AVHRR and MODIS observations with biome-

216   specific LAI-VI relationship[54-56], while global leaf chlorophyll content was firstly generated from

217   MERIS observations by physically-based radiative transfer models instead of the chlorophyll-

218   sensitive MTCI, due to the impact of LAI on MTCI[57]. For very high spatial resolution (<10-m),

219   GeoEye-1, WorldView 2-4, Pleiades, SkySat and PlanetScope are available since 2009 but can

220   only provide VIS-NIR reflectance for vegetation biophysical properties. DESIS and HiSUI on the

221   International Space Station, and as well as Hyperion and PRISMA, provide the hyperspectral

222   observations while they just have monthly revisit cycle on average, which are suitable for plant

223   biochemical and physiological traits mapping instead of capturing rapid temporal changes of

224   vegetation.

4. Ecological applications of VIs

225

226   VIs have been successfully applied to many specific ecological research fields. Below we

227   discuss a few prototypical examples.

228   *4.1 Estimating vegetation attributes*

229   An essential attractive feature of VIs is their conceptual simplicity and strong relationships

230   with vegetation biophysical properties. Therefore, using VIs to estimate vegetation biophysical

231   properties such as LAI, fractional vegetation cover, and biomass[54,55,58] is one of the most successful

232   application scenarios. Many VIs such as NDVI have been used as robust estimators of LAI and

233   fractional vegetation cover. A few problems of NDVI are well identified, such as the insensitivity

234   to densely vegetated areas and the oversensitivity to the changes of soil brightness due to rainfall

235   and snowfall. The saturation point of EVI is higher than NDVI[25,27], leading to more EVI

236   applications in densely vegetated area like tropical forests. In particular, chlorophyll-corrected VIs

237   can minimize the impact of chlorophyll content on LAI estimations. For example, a modified

238   triangular vegetation index (MTVI2) and a modified chlorophyll absorption ratio index (MCARI2)

239   have shown to be the best predictors of green LAI in a systematic evaluation of more than ten VIs

240   (including NDVI, MSR, SAVI, etc.) over various crops[59].

241   For vegetation biochemical properties (Table 1), red-edge VIs have been widely used for

242   estimating leaf/canopy chlorophyll content and carotenoid pigments[60], while SWIR-based VIs were

243   often roughly used for leaf/canopy water content, leaf mass per area and (LMA) and nitrogen

244   estimations[32]. These retrieved plant traits can be directly used to quantify the functional diversity,

245   while the spatial distribution and textural feature of VIs such as MODIS EVI have also been

246   applied in studying the spectral diversity, species richness and habitat heterogeneity[61,62].

247   *4.2 Temporal vegetation dynamics*

248   Compared to other VIs, NDVI and EVI are the most widely used ones in practice for detecting

249   and monitoring temporal vegetation dynamics because of their simplicity, robustness and

250   availability, especially for the seasonal (phenology) and long-term trends of structural changes [7,63-

251   [65]. EVI and EVI2 are the primary data source for producing the MODIS vegetation phenology

252   product Collections 5 and 6, respectively. In the recent years, NIRv is gaining popularity for

253   analyses of vegetation changes regarding the ecosystem gross primary production (GPP)[66]. PPI and

254   EVI2 performed better than NDVI with Sentinel-2 imagery across Europe when compared to

255   ground-observed phenological stages, especially for evergreen coniferous forest during winter with

256   snow[67]. CCI better tracked evergreen forest phenology and the end-of-season changes in deciduous

257   forests compared to structurally-oriented NDVI, EVI and NIRv[68].

258   Artifacts such as sun-sensor geometry and inter-sensor calibrations usually play a critical role

259   for correctly using and interpreting the results of VI-based temporal vegetation dynamics. During

260   the past decades, considering the inter-sensor consistency and the sun-sensor geometry has been

261   well recognized by the research community although different VIs may subject to such artifacts at

262   different levels of sensitivities as discussed in Section 5.

263   *4.3 Environmental stresses and disturbances*

264   The abrupt temporal changes of VI time-series are also useful for the detection of land cover

265   change, environmental stress and disturbance. EVI has been widely used to monitor and quantify

266   the deforestation and degradation in the Amazon tropical rainforest[69], as well as the responses to

267   drought, heatwave and water stresses[10,11,70]. Using PRI, CCI and GCC infers more seasonal

268   physiological changes of vegetation than using structurally-oriented VIs such as NDVI and EVI in

269   dormant temperate forests[50,51]. Biochemically-related VIs such as SIPI, NPCI and ARI have also

270   been applied for the detection of pests and diseases in winter wheat[71], and the soil erosion and

271   heavy metal pollution in rice[72], especially when hyperspectral data are available. Forecasting

272   wildfire risks, monitoring fire severity, and characterizing vegetation recovery after fire

273   disturbance is typically achieved by simple VIs such as NDVI, while hyperspectral imaging

274   spectroscopy and light detection and ranging (LiDAR) are encouraged to be used in combination

275   for the assessment of fuel condition and vegetation structure mapping[12]. NDVI has also been used

276   for the assessment of ecosystem integrity and land degradation/desertification at different scales,

277   including the resilience of agroecosystems[73].

4.4 Ecosystem carbon and water fluxes

Vegetation dynamics drive changes of surface radiation regime, which co-determine microclimate and land-atmosphere carbon and water fluxes, and thus has been an important application of VIs, in principle by employing VIs as the proxy for vegetation canopy coverage, leaf area and fraction of absorbed solar radiation (FPAR) (Fig. 3). FPAR is usually considered as a function of LAI, and thus the advantages and disadvantages of the VIs for monitoring LAI also apply to the carbon fluxes estimations.

Some notable examples of using VI to estimate carbon fluxes, particularly GPP, include the Carnegie-Ames-Stanford Approach (CASA)[74], MODIS algorithm[75] and EC-LUE model[76] (all using NDVI-derived FPAR); Vegetation Photosynthesis Model (VPM)[44], the modified GPP model in TEM[77], data-driven GPP upscaling[78] (using EVI); simpler statistical upscaling using NIRv[30,79]; regional forest GPP estimations[80] (using EVI2); satellite-based GPP with inexplicit parameterization of LUE[6,79] (using NDVI and soil-adjusted NIRv, SANIRv). All these approaches have demonstrated moderate to high success. NIRv has received growing attention in recent years because of its explicit physical link to FPAR[30,81,82] as well as a moderate relationship with LUE[83]. PRI, CCI and GCC are also found to well track the seasonal GPP dynamics, it is still challenging to establish quantitative relationships between these VIs and LUE for robust GPP estimations. Nevertheless, the inclusion of PRI together with NDVI had shown improvements in estimating boreal forest CO_2 fluxes [84].

VIs have been used as direct indicators of photosynthesis in studies, such as for examining the CO_2 fertilization effects by using AVHRR and MODIS NIRv[85,86], the carbon loss in Amazon rainforest degradation and deforestation with MODIS EVI[69], the change velocity and optimum air temperature of productivity across biomes by MODIS NDVI and NIRv[87], and the anomalies and recovery of the tropical forest during the strong 2015/2016 El Niño event also with MODIS EVI[88,89]. Estimating belowground carbon fluxes from satellite observations has rarely been attempted and is based on indirect correlations between GPP and soil respiration via VIs[90].

304 Typically, NDVI, EVI and MSAVI were used as scaling factors to extrapolate field-level soil

305 respiration measurements to larger scales [90,91].

306   Another prominent application of VIs is in the estimation of evapotranspiration (ET) with a

307 history of over 30 years[92,93]. Although ET has been more accurately assessed using land surface

308 temperature (LST), VIs are easier to obtain. The principle is because transpiration through plant

309 leaf stomata generally dominates evaporation. A number of previous review papers have

310 summarized that VIs in remote sensing ET models are powerful indicators of the fraction of

311 vegetation coverage, absorption of solar energy, or surface roughness that are major determinant of

312 ET[94,95]. Besides, due to the good VI-LST or VI-ET correlations observed at the flux tower sites in a

313 wide variety of ecosystems, VIs have been used for either up-scaling site observation or

314 enhancing/downscaling satellite LST, especially when LST data is unavailable or has a coarse

315 resolution[94,96]. NDVI, SAVI and EVI are so far the most widely used VIs in a variety of ET

316 estimation models[95-97]. However, due to NDVI's sensitivity to soil brightness, the more soil-

317 resistant VIs, such as EVI, EVI2, NIRv and SAVI, are considered as better choices[92,94,96].

318 **5. Artefacts that cause inconsistencies**

319   VIs can be easily acquired from a variety of satellite sensors, however, inconsistencies in VI-

320 based results reported in literature are common. Some of these inconsistencies are due to the use of

321 different VIs, and a majority others are due to the artefacts of VI products derived from different

322 sensors, satellite product versions, atmospheric and directional correction effects, compositing

323 algorithms, and the application of different levels of quality assurance (QA) and quality control

324 (QC) flags[70]. A comprehensive understanding of these inconsistencies as well as the limitations and

325 caveats of each VI is critically important for rigorous use of VI and for the correct interpretation of

326 the results from VI-based analyses. In this section, several notable examples of how VIs are not

327 used consistently are discussed and classified by the primary factors for such inconsistencies (Fig.

328 4).

329 *5.1 Sensor and calibration effects*

There are inconsistencies in different satellite time-series for the same study area/region. For example, vegetation greenness trends derived from AVHRR and MODIS NDVI time series apparently show trends in opposing directions[98]. The differences in the central wavelength and range of the spectral response function across sensors can be important contributing factor for such inconsistencies[99,100]. For example, NDVI obtained from AVHRR, MODIS, and VIIRS show significant differences in values and the level of the differences varies across land cover types, although their orbits and spatio-temporal resolutions are similar[9].

Besides, satellites and their sensors often suffer from the harsh space environment, resulting in orbital drift and sensor degradation over time. Although onboard calibration or vicarious calibration are applied to maintain the measuring standards, the remaining limitations can affect the accuracy of the derived VIs and introduce systematic biases especially in long-term trend analyses[101,102]. Typical examples involve products from AVHRR and MODIS[103,104]. AVHRR measurements come from a series of satellites, each of which has specific orbital characteristics[105,106] which can affect the image acquisition time and sun-target-sensor geometry[104]. In particular, NDVI values from AVHRR onboard NOAA-11 were found to be significantly higher than those from prior and subsequent AVHRR sensors[107]. Orbital drift effects were also found in the VIP3 and LTDR4 NDVI data and over the more humid areas for GIMMS-3g NDVI. MODIS-based NDVI exhibited an increasing trend during 2001~2016, while a decreasing trend of the GIMMS-based NDVI was observed especially after 2012, which suggests large discrepancies of global greening[108]. A significant positive jump in the SPOT-VGT NDVI time series was identified due to the platform/sensor change from VGT-1 to VGT-2[8]. A recent study used AVHRR NIRv as a long-term consistent record to quantify the trends in CO_2 fertilization effect on global vegetation photosynthesis from 1982 to 2015[85]. However, concerns were raised about potential uncertainties in the conclusion partly due to sensor differences[86,104].

Another important issue is that different VIs may show varying levels of sensitivity to sensor calibration due to their mathematical formulae. The calibration bias may affect both VIS and NIR bands in a similar way, and thus can at least partly cancel out in ratio-based VIs such as NDVI and

357 SR. For example, the single-band reflectance calibration uncertainty for MODIS was 2% under

358 normal atmosphere conditions, while the mean NDVI uncertainties due to sensor calibration was

359 only ± 0.01 units and was less than 2% of the dynamic range using field canopy reflectance

360 observations[109]. The cross-sensor difference of NDVI could also be smaller than the difference of

361 surface reflectance. For the comparison among fifteen moderate-resolution sensors including

362 MODIS, VIIRS and AVHRR, each pair of the sensors had a larger R^2 and smaller Root Mean

363 Square Error (RMSE) for NDVI than for the VIS and NIR bands separately[9]. In VIs such as NIRv

364 (=NDVI×NIR), such calibration biases do not cancel out and thus can impact the absolute values of

365 the VI signals as NIR reflectance is multiplied. While this could be problematic for applications

366 that rely on the absolute values of VI, it could also be an issue for the consistency of long-term

367 time-series when there are differences in calibration bias between different sensors, or calibration

368 drift of a given sensor over time. Therefore, differences in vegetation trends and magnitudes for

369 different VIs can be due not only to the inherent characteristics of the VIs but also to their different

370 sensitivities to calibration bias.

371 *5.2 Product versions*

372 VIs satellite products are usually produced in different versions (collections) with algorithmic

373 improvements and calibration adjustments. Using different VI product versions may lead to

374 inconsistent interpretation of changes in the vegetation. There still exist inconsistent

375 greening/browning trends between MODIS Collection 5 (C5) and Collection 6 (C6) products[102].

376 MODIS itself suffers from sensor degradation, which is the largest for the Terra satellite especially

377 in the blue band[102,110]. The degree of degradation decreases with increasing wavelength, and thus

378 there are negative decadal trend artefacts for MODIS Terra products with △NDVI~0.01 and △

379 EVI~0.02[110] when comparing C5 to an enhanced C6 (C6+) version. The percentage of negative

380 MODIS-C5 NDVI trends derived from Terra (17.4%) was nearly three times as large as that

381 derived from Aqua (6.7%) for North America during 2002~2010[101]. Most of the vegetation

382 browning trends revealed by MODIS Terra-C5 VIs were likely caused by sensor degradation,

383 particularly during the period after 2007, and thus previous studies of vegetation trends based on

384   only Terra-C5 VIs may need to be re-evaluated[102]. Thus the latest MODIS C6 has sensor

385   degradation corrected and better consistency between Terra and Aqua measurements and provides

386   a more reliable record than C5[110].

5.3 Pre-processing steps

388   Standard VI products usually include important data pre-processing and sensor configuration

389   information, such as the sun-target-sensor geometry and QA/QC, which if not taken into account

390   appropriately, could introduce critical errors in the subsequent analyses. The relative positions of

391   the sun, sensor and observing target commonly change over time due to the continuous movement

392   of Earth, sun, and satellites. Such changes result in the variations of the solar illumination and

393   sensor viewing angles and have been recognized for decades to affect remotely sensed observations

394   strongly[111-113]. This effect can be mathematically described as the bidirectional reflectance

395   distribution function (BRDF) effect or the sun-target-sensor geometry effect (Fig. 4).

396   The solar angle is seasonally and latitudinally varying but annually repetitive if a sensor

397   remains in a stable orbit, and therefore it can influence the VI-based phenology, but not the long-

398   term trends or interannual variations. For example, Amazon forests have been reported to exhibit

399   no variations in EVI from wet to dry season, and dry season greening has been attributed to

400   seasonal solar-angle variations[112]. Subsequent studies using either the same data[114] or the

401   rigorously BRDF-corrected MAIAC product[115] suggested dry-season greening but with smaller

402   magnitude, which demonstrates the importance of disentangling solar angle-induced seasonal

403   variations in VI from vegetation-induced variations. A similar case also shows that the BRDF

404   effect, instead of the vegetation response, drives the satellite NDVI phenology in evergreen sparse

405   canopy ecosystems in western US with subtle growth dynamics[116]. Not only MODIS, but also

406   Landsat 7, Sentinel-2, VIIRS and Proba-V confirmed this effect with the ground-based PhenoCam

407   observations as the reference. Thus the authors suggest to either restrict the analyses to selected

408   data with consistent sun-target-sensor geometry, or to rigorously remove the BRDF effect in the

409   data[116]. Landsat that only acquires images at ± 7.5° from nadir has relatively small view angle

410   effects[117], while other satellite sensors such as AVHRR and MODIS usually extend to larger view

411 angles, which can introduce uncertainties to the downstream products if uncorrected[111,113]. The

412 impact of the BRDF effect on MODIS NDVI was evaluated in West Africa, and was found to be

413 the highest for medium dense vegetation (NDVI≈0.5~0.6) compared to sparsely canopy

414 (NDVI≈0.3~0.35) or dense vegetation (NDVI≈0.7)[113]. In Alaska Arctic tundra, the influence of

415 BRDF effect on satellite NDVI-based biomass estimations was up to 33% (excluding extremes)

416 more sensitive than on NDVI[111].

417 A related uncertainty source is the compositing approach, which determines how to extract the

418 highest quality observations over the typically used 8-day, 16-day, or monthly interval.

419 Compositing has gone through major changes between the traditional Maximum Value

420 Compositing (MVC) algorithm, which is still employed in GIMMS-3g datasets, to the modified

421 constrained view angle MVC, or CV-MVC[25], used in MODIS VI compositing (MOD13A1 and

422 MYD13A1), to the 16-day rolling compositing based on BRDF retrievals used in MCD43A4 Nadir

423 BRDF-Adjusted Reflectance (NBAR)-VIs[118]. Note that MOD13A1 and MYD13A1 products with

424 the CV-MVC algorithm aimed to reduce the BRDF effect but still did not theoretically normalize

425 it[119], while the MCD43A4 C6 product removed the view angle effects but was set at the local solar

426 noon zenith angle[120] which varies seasonally and latitudinally. Compositing approaches vary

427 widely and can lead to inconsistencies in the interpretation of results. For example, in the studies

428 conducted over the Amazon[63,70,121] and western US[116], selective compositing settings based on

429 study objectives resulted in inconsistent results.

430 Another source of inconsistency is the atmospheric correction, which was either conducted

431 fully, partially or sometimes not at all conducted for different VI products. MODIS attempted the

432 full correction, while GIMMS attempted at limited correction. NDVI derived from VIIRS

433 observations is based on top-of-atmosphere (TOA) reflectance, while VIIRS EVI is generated

434 based on surface reflectance[122]. Even when VIs are calculated from atmospherically-corrected

435 reflectance at the surface, they are still subject to uncertainties in atmospheric correction such as

436 cloud masking, residual sub-pixel clouds, incomplete corrections for Rayleigh scattering, ozone,

437 water vapor absorptions, and imperfect aerosol correction[123]. In the studies regarding the impact of

438 drought on Amazon forests, where VIs were intensively used, large differences were found in the

439 extent of Amazon greening during the 2005 drought that were attributed to inadequate QA/QC

440 screening for clouds and aerosols effects that are usually accounted for in atmospheric correction

441 process[70].

442 *5.4 Soil, snow and topographic effects*

443 Most of Earth's terrestrial ecosystems have sparse canopies with appreciable canopy

444 background (soil, litter, snow, water, etc.) signals that can affect satellite-derived VIs. Soil types

445 and soil moisture conditions lead to spatiotemporal variations of soil brightness[124]. In natural

446 ecosystems, the soil layer could be mixed with litter, moss, lichen, or waterbodies; and especially

447 in forest ecosystems, woody stems and branches could contribute to the background noise or bias

448 of VIs[125]. Soil influences are assumed to vary the most in arid regions, while they have the greatest

449 effect in moderately vegetated canopies (LAI ~1 or ~50% cover). For example, in northern Africa,

450 extensive soil-artefacts in the AVHRR-NDVI signals are seen over reddish soils[126], while in the

451 Sahel, the NDVI variations were reported due to soil type, moisture and reflectance differences[127].

452 The first rains can result in an artefact NDVI flush prior to the actual greening cycle, while over-

453 irrigated and freshly ploughed croplands, one can see similar NDVI 'soil artefacts'[128]. Snow and ice

454 with high optical reflectance are among the most important factors that lead to the inconsistency of

455 the VI time-series during winter in temperate regions[116,129] or, more permanently, in Arctic[130].

456 There is evidence of bias in the detection of vegetation phenology phase using NDVI at the end of

457 non-growing season, due to presence of snow that causes low NDVI values[131].

458 In addition to soil and snow, topography also influences VIs. Mountainous regions cover 24%

459 of the total Earth's land surface[132]. Topography, which can cast macro-scale shadows and change

460 the local sun-surface-sensor geometry, has been reported to have important effects on surface

461 reflectance[133] and VIs[134]. Similar to the shadows in view caused by the sun-target-sensor geometry,

462 a topographic shadow is much darker in the red wavelength than in highly scattered NIR

463 wavelength due to the multiple scattering between slopes[135]. Compared to the sun-target-sensor

464 geometry-induced porous and fuzzy canopy shadows, the dark and opaque topographic shadows

465   can have larger effects on EVI[134]. The topographic effects on reflectance should be minimized

466   before EVI and other VIs without a band-ratio format (such as NIRv and SAVI) are calculated,

467   while the topographic effects on the ratio-based VIs such as SR and NDVI are usually smaller[134].

468   The topographic effects are also related to the spatial scale and as the size of the pixel increases,

469   the topographic effects may decrease and even disappear with spatial averaging[136].

470   *5.5 Scale-mismatch effects*

471   Spatial mismatches between the region-of-interest and the predefined grid cells in the remote

472   sensing-based datasets could be another important source of uncertainty[137]. For example, MODIS

473   pixels have accurate geolocation, yet on average, the offset is up to half a pixel between scenes,

474   which is significant when users rely on single pixel VIs to match with *in-situ* measurements[138].

475   Considering that the *in-situ* measurement is rarely near the centre of a pixel, there is high

476   probability that a single MODIS pixel may not always sample the *in-situ* measurement area. The

477   sensor point spread function could further distort the matching of gridded satellite data with

478   ground-based data[137]. The emerging high-spatial resolution data (for example, PlanetScope and

479   airborne data, ≤ 3 m) could also lead to difficulties in the interpretation. For example, a pixel could

480   be completely in the shadows of a tree so that VI values could be highly distorted due to the lower

481   illumination than sunlit crown side if the research target is the whole tree canopy[139]. Identifying a

482   suitable remote sensing product at an appropriate spatial scale could be the most effective choice

483   for minimizing such uncertainties.

484   There is a general lack of studies that use long-term, well-coordinated *in-situ* networks to

485   measure reflected radiation from vegetation to confirm larger scale greening and browning results.

486   The MODIS EVI results related to the Amazon dry season greening were confirmed with *in-situ*

487   measurements of GPP from eddy-covariance flux towers[140]. In contrast, the greening trends in the

488   Sahel challenge the mainstream paradigm of irreversible ground-observed land degradation in this

489   region[141]. There is also a debate as to whether the onset of spring phenology has been advancing

490   due to climate warming. The trends in the Start Of growing Season (SOS) for Tibet alpine meadow

491   and steppe were examined using ground-based phenology observations as well as NDVI datasets

492 from GIMMS and GIMMS3g, MODIS, SPOT-VEG and SeaWiFS[142]. The results from that study

493 showed large discrepancies in the SOS trends among the ground-based and different NDVI

494 datasets, and between the different phenology retrieval. The study pointed out the NDVI data

495 quality and scale-mismatch between satellite and ground data might be an important reason for

496 these inconsistencies. Similar results were reported by comparing ground-based PhenoCam data

497 with EVI derived from a variety of sensors including Landsat ETM+, MODIS, and DSCOVR-

498 EPIC[65]. At three rural sites and one urban site of deciduous trees in Ireland, AVHRR and MODIS

499 EVI2-derived SOS during 1982~2016 was consistently earlier than *in-situ* leaf-unfolding across all

500 these sites with the RMSE of 25~52 days and Mean Bias Error (MBE) of −5 to −50 days, while

501 satellite-derived growing-season-length was consistently longer than *in-situ* data with the RMSE of

502 65~102 days and MBE of 45 to 96 days[143]. For the period 2001~2014, MODIS EVI2-derived SOS

503 advanced by about 2.36 days from middle to high latitudes of Northern Hemisphere

504 (43.5°N~70.0°N) snow-covered landmass, while delayed by about 0.53 days in lower latitudes

505 (33.0°N~43.5°N); the differences between MODIS EVI2-derived SOS and *in-situ* SOS at 420

506 phenology observations from five filed datasets including Pan European Phenology (PEP)

507 project[144,145] are centralized between −30 days and 30 days, with the coefficient of determination

508 (R^2) of 0.67, RMSE of 12.13 days and bias of −3.99 days[146].

509 **6. Limitations and intrinsic linkage**

510 *6.1 Notable limitations of VIs*

511   In principle, VIs capture a combination of canopy properties and other external contributing

512 factors such as atmospheric conditions and sun-target-sensor geometry that may simultaneously

513 and non-uniquely vary throughout the vegetation growing season. Thus, it might be infeasible to

514 physically couple a VI to a specific plant variable without accounting for changes due to these

515 factors and changing vegetation conditions at the same time. For example, a VI cannot be coupled

516 to leaf biomass, without accounting for simultaneous differences in leaf biochemical constituent

517 differences, non-photosynthetic vegetation (NPV), soil background, atmospheric contamination,

518 and canopy structural effects, which are also tightly connected to the sun-target-sensor geometry

519 effects. From the mathematical formula, a large group of ratio-based VIs (e.g., NDVI, SR, PRI,

520 CCI and CIred-edge), are sensitive to different soil brightness due to the larger variation of the

521 denominator than the numerator[2], but are insensitive to fractional vegetation cover when the soil

522 background is dark or in water for mangrove[147]. For example, a leaf floating in a black water body

523 would maintain the same NDVI regardless of how large the leaf became (whether that leaf

524 occupies 1% of the water or 100% of the water, the NDVI is the same, as in Fig. 4).

525 Impacts of some inherent properties of vegetation, such as the leaf biochemical constituents

526 and NPV, are usually difficult to separate because of limited understanding of their spatiotemporal

527 variations. Leaf biochemical constituents, such as chlorophyll, water and dry matter contents,

528 largely determine the leaf reflectance spectrum and thus fundamentally shape the vegetation

529 canopy reflectance[148,149]. Recent studies have demonstrated the strong spatio-temporal variations of

530 leaf biochemical constituents[57,150], which contribute to the important plant diversity but greatly

531 complicate the interpretations of VIs. NPVs, such as woody stems, branches, and standing litter[151]

532 can mask emerging green vegetation and thus can weaken the correlation between VIs and green

533 vegetation biophysical properties. Therefore, satellite-derived phenology could be delayed due to

534 the masking of NPVs, because the standing plant materials from the previous year may occlude the

535 initial green-up of vegetation[151]. The limitations of VIs can be at least partially addressed when the

536 VI formulae are appropriately designed with the principles of radiative transfer in vegetation

537 canopies (Section S2.2).

538 *6.2 Intrinsic similarities between VIs*

539 Red-NIR VIs , such as NDVI, DVI, EVI, EVI2 and NIRv, are typically among the most

540 widely-used category. In general, surface reflectance in NIR band is larger than that in the red band.

541 In addition, canopy NIR reflectance essentially increases with LAI while red reflectance shows the

542 opposite trend due to strong light absorption at this wavelength. Therefore, NIR typically

543 dominates the factor NIR/(NIR+Red), which equals NIRv/DVI. It typically falls in a small range of

544 0.8~1 for vegetated surfaces (LAI>1). Therefore, Eq. 2 in Box 1 suggests that NIRv is well

545   correlated with DVI in most cases, and NIRv has the biophysical meaning of FPAR times photon

546   escape probability (*fesc*) (Fig. 3a).

547   EVI has been reported to be well approximated by EVI2, a variant of EVI without the blue

548   band[27]. EVI and EVI2 can be derived as the product of DVI and $2.5/(NIR+6 \cdot Red+7.5 \cdot Blue+1)$ or

549      $2.5/(NIR+2.4 \cdot Red+1)$ (Eqs. 3-4), respectively[27]. Note that the number '1' in the denominator is

550   typically much larger than the variability of the remaining term $(NIR+2.4 \cdot Red)$ or

551      $(NIR+6 \cdot Red+7.5 \cdot Blue)$ in response to the changes of LAI. Thus, the factor

552      $1/(NIR+6 \cdot Red+7.5 \cdot Blue+1)$ (Eq. 3) is typically between 0.7~0.8 in most cases especially when

553   LAI is greater than 1. Similarly, the factor $1/(NIR+2.4 \cdot Red+1)$ is also almost a constant with small

554   variation between 0.7~0.8 in most cases. This suggests that EVI2 and EVI should have a strong

555   linear correlation with DVI, although with different magnitudes because of the constant coefficient

556   (2.5) used in the numerator.

557   Thus, DVI is strongly correlated to both EVI and NIRv, and NIRv, DVI, EVI and EVI2

558   intrinsically have strong linear correlations with one another according to their mathematical

559   definitions and typical range of variation of NIR and VIS reflectance of vegetated surfaces. In

560   contrast, DVI is mathematically the numerator of NDVI, and the denominator (NIR+Red) can vary

561   significantly with LAI and other vegetation properties. Therefore, a nonlinear relationship is often

562   observed between NDVI and DVI, and thereby also between NDVI and the other indices similar to

563   DVI, such as EVI, EVI2 and NIRv.

564   NDVI, EVI and DVI can also be more generally described by another well-known VI, the

565   SAVI, and the 'L' in the denominator of SAVI (Eq. 7) is the canopy background adjustment term

566   that addresses the nonlinear, differential NIR and red radiative transfer process through a canopy[3,25].

567   In case L in SAVI is 0, SAVI is equal to NDVI; if L is 1, SAVI equals to EVI. Note that factors of

568   6 and 7.5 in the denominator of EVI (Eq. 3), and 2.4 in the denominator of EVI2 (Eq. 4), are for

569   atmosphere self-correction instead of canopy biophysical properties. Third, when L is infinity,

570   SAVI is equal to DVI. The real canopy has an L value generally greater than 0 but less than 10.

571   Details about the evaluation of similarity and difference among these VIs, and their sensitivity to

572   artefacts such as the impacts of soil background, atmospheric contamination, canopy structural and

573   sun-target-sensor geometry effects are in Section S2.1.

574   **7.   Appropriate use of VIs**

575   Attractive features of VIs are their conceptual simplicity and strong relationships with target

576   properties of the vegetation and land cover. Because of the diverse types and application scenarios

577   of VIs, it is not possible for a universal recommendation of the best VI. Instead, identifying the

578   target application and corresponding sensitive wavelength and VI is the first step towards the

579   optimal use of VIs. For example, red-NIR VIs such as NDVI and EVI may be the best choices for

580   studying dynamics of vegetation structure, red-edge VIs are more suitable for pigment retrievals,

581   while VIS-based PRI and CCI are more appropriate for the monitoring of physiological changes.

582   Then, understanding the intrinsic differences, strengths and particularly the limitations of VIs may

583   help to further identify the suitable VIs. For example, NDVI may be the best candidate VI for

584   estimating fractional vegetation cover as it is less impacted by sun-target-sensor geometry than

585   EVI and NIRv, while if the sun-target-sensor geometry effect is properly addressed, NDVI may be

586   less robust in estimating fractional vegetation cover due to the stronger sensitivity to soil brightness

587   changes from rainfall or snowfall[2,3]. In addition, VIs are typically saturated in dense vegetated

588   areas; the saturation point of NDVI is usually lower than EVI[25,27], suggesting that NDVI may be a

589   less appropriate choice for analysing vegetation variations in dense vegetation canopies, while

590   NDVI is still useful for onset/offset phenology detection. Even though EVI, EVI2, DVI and NIRv

591   show high correlations, the mechanistic link that was established between NIRv and the product of

592   FPAR times *fesc* (Fig. 3) makes NIRv an attractive choice for studies related to GPP estimation

593   and SIF[81,83,152,153].

594   Potential artefacts must be carefully taken care of to avoid biased interpretations of the

595   underlying ecological processes resulting from the use of the incorrect data. Due to sensor

596   degradation, the analysis and interpretation of the interannual variations and long-term trends in

597   VIs remained challenging until the inter-calibration of AVHRR with MODIS became feasible after

598   2000 during the overlapping period[103]. The newer versions of VI products should theoretically be

599   more accurate than the older ones[110]. Spectral response function normalizations are recommended

600   for multi-sensor VI harmonizations[99]. The BRDF correction by the kernel-driven model is

601   recommended especially if the BRDF varies seasonally and latitudinally in the analysis[120]. If

602   uncertainties from sensor calibration[109], atmospheric, BRDF and topographic effects[134] are a

603   serious issue to be reduced, ratio-based VIs are more recommended than difference-based VIs,

604   while ratio-based VIs could be sensitive to snow/soil background[130] and scale effects[58]. For the

605   spatial aggregation, it is highly recommended to firstly aggregate the single-band reflectance to

606   coarse resolution, and then calculate VIs such as NDVI and EVI, instead of aggregating the high-

607   resolution VIs directly, just to avoid the scaling effect over heterogeneous surfaces due to possible

608   nonlinear formula of VIs[58].

609   Identifying dominant variables and potential signal contamination sources in specific

610   ecosystems are also important for the correct use of VIs. For example, for temperate evergreen

611   forests, the structure and chlorophyll in winter may not vary much, while physiologically-

612   associated VIs such as PRI and CCI which are more sensitive to light use efficiency should be

613   more suitable[50,51]. Tropical rainforest could be more vulnerable to atmosphere and optical signal

614   saturation impacts[114] (EVI is more recommended instead of NDVI), savanna and shrubland with

615   sparse vegetation are more sensitive to soil backgrounds[25] (EVI and NIRv are recommended), Artic

616   region with high latitudes is vulnerable to large solar zenith angle and ice/snow backgrounds[130]

617   (PPI, EVI2 and NIRv with BRDF correction are recommended), while mountainous regions such

618   as the Tibetan Plateau with rugged terrain is vulnerable to not only ice/snow but also topographic

619   and shadowing effects[142] (topographic normalizations including the empirical, semi-empirical and

620   physically-based methods[154] are recommended).

621   **8. Future directions**

622   VIs with the spectral, angular, spatial and temporal information are classic remote sensing

623   products with rich research history. Because of their simplicity and robustness, we envision they

624   will continue to be heavily used in the foreseeable future. Looking forward, we identified a few

625   research opportunities and challenges below that may advance the use of VIs for the more accurate

626   and timely monitoring of terrestrial ecosystems from space.

627   *8.1 Multi-sensor VI harmonization*

628   Multi-sensor fusion of observations from multiple sensors/satellites can improve the spatio-

629   temporal resolution and continuity as well as the timespan of VIs, such as Sentinel-2 and Landsat-

630   8[155], which may greatly enhance their applicability. Ongoing efforts are devoted to developing

631   fusion algorithms[156-159] and datasets[118,160,161] for producing long-term gap-free VIs at relatively high

632   resolutions. However, land surface heterogeneity[162] and BRDF effects[117] remain to be major

633   scientific challenges and issues to be resolved for producing fused VI products. The atmospheric

634   correction also deserves greater attention, because even under the same solar angle, VIs differ

635   depending on the fraction of diffuse radiation which differs at the overpassing times of different

636   sensors/satellites. Sensor calibration drift and degradation are also critical challenges for the fusion

637   of VI data from similar sensors on multiple satellites or multiple sensors on different satellites such

638   as AVHRR and MODIS, in producing decadal datasets and analyses[103,104].

639   *8.2 Synergistic use with novel metrics*

640   Most VIs are good proxies of vegetation biophysical properties and to a limited extent

641   represent vegetation functioning. Some novel remote sensing indicators, such as Solar-Induced

642   chlorophyll Fluorescence (SIF)[163-166], could provide valuable complementary information. SIF

643   captures some of the vegetation physiological information, and thus responds to the onset of

644   environmental conditions and stresses earlier than VIs[167]. SIF can track the photosynthetic

645   seasonality in evergreen species in cold environments where red-NIR VIs showed no changes[168].

646   Besides, SIF is rarely impacted by soil because green vegetation is the only source of SIF.

647   However, the existing SIF retrievals have poor spatial resolution, infrequent revisiting time,

648   low signal to noise ratio, and a relatively short history of measurements[169]. New sensors/satellites

649   will continue enhancing the capability for SIF measurement, but complementary VIs such as NIRv

650   provide far better spatial and temporal resolutions. Understanding the intrinsic linkage between SIF

651 and VIs is the key for the synergistic use for scientific applications, and one possible useful

652 direction is to study the shared characteristics of SIF and VIs. In recent studies, far-red SIF

653 normalized by Photosynthetically Active Radiation (SIF/PAR) and NIRv has been demonstrated to

654 share the same *fesc* in the radiative transfer process[81,170] (Box 1). Thus, under low-stress conditions

655 with stable fluorescence yield (Φ_F), NIRv and SIF/PAR are expected to be strongly correlated

656 under the same sun-target-sensor geometry (Fig. S1). NIRv radiance (NDVI×NIR radiance) or

657 NIRvP (NIRv×PAR) and SIF should be even more strongly related than NIRv and SIF/PAR as the

658 common radiation factor further enhances the underlying relationship[4,82,152]. The similarity between

659 NIRv and SIF implies that VIs could be used as structural proxies for SIF because they have a

660 longer data record. For example, MODIS EVI has been used to generate a global SIF product

661 (GOSIF; 2000-2020) from OCO-2 SIF soundings[171]. Combining NIRv with SIF during times of the

662 overlapping data has great potential to isolate the unique physiological responses of SIF as NIRv

663 can be used to normalize the dominant canopy structure effects[152,172].

664 Microwave vegetation indices derived from different frequency and polarization combinations

665 are more sensitive to the woody part of the vegetation than NDVI[173], and are potential approaches

666 to derive vegetation optical depth (VOD)[174]. VOD describes vegetation extinction effects in the

667 microwave spectrum and is increasingly used for estimating parameters of vegetation water content

668 and the aboveground biomass[175,176]. VOD has the advantage of being unaffected by the clouds and

669 less sensitive to the water in the atmosphere, which is important especially for cloudy and humid

670 tropical regions such as the Amazon and Congo rainforests[175,177]. VOD has been reported to have a

671 saturation point with higher biomass values than NDVI[177]. Optical VIs with a higher spatial

672 resolution can contribute to the downscaling of VOD, while VOD can help to improve the

673 temporal observing frequency over cloudy and humid regions and seasons.

674 *8.3 New remote sensing missions*

675 The widely used red-NIR VIs which are sensitive to canopy structure and chlorophyll content

676 do not directly contain the LUE information, which can be captured to some degree by several VIs

677 such as PRI[49], CCI[5] and GCC[50,51] from emerging hyperspectral or multispectral remote sensing

678   capabilities. In addition, hyperspectral data with more spectral information can be beneficial for the

679   disentangling of the pure vegetation and soil reflectance contributions in the mixed pixel spectrum,

680   by the newly proposed NIRvH[153]. The next generation of VIs aim at the reduction of soil/snow/ice

681   background effects, reduced BRDF impact and reduced signal-saturation. Such hyperspectral

682   remote sensing capability has been limited at the global scale and relatively fine spatial resolution.

683   However, these limitations will be addressed with the emerging and forthcoming spaceborne

684   hyperspectral satellite missions such as the HiSUI, PRISMA, EnMap, CHIME, DESIS, GeoCarb

685   and SBG. New opportunities to further improve temporal characteristics of traditional VIs will also

686   be provided by the new-generation geostationary satellites, such as GOES, Himawari and GEO-

687   KOMPSAT, as well as the unique DSCOVR position at the Sun-Earth L1 Lagrange Point. They

688   provide higher observing frequency that support not only the diurnal variations of ecosystem

689   processes[178], but also the seasonality of greenness in cloudy and humid regions such as Amazon

690   compared to polar-orbiting satellites[179,180].

691   **9. Summary**

692   This review summarizes inherent features of several widely used VIs and some factors

693   contributing to consistencies and inconsistencies among them that may lead to controversies

694   resulting from their inappropriate use in scientific studies and other applications. Factors such as

695   the formulation of VIs, sensor characteristics, product version, compositing algorithms, QA/QC,

696   atmospheric and topographic conditions, and sun-target-sensor geometries all impact VIs and their

697   appropriate use. We further highlight that improper use of QA/QC flags attached to VIs could be

698   an important source of uncertainty and pitfall in their use, and offer a few guidance and

699   recommendations for the appropriate use of VIs. Mathematical analysis suggests that NIRv, EVI,

700   EVI2 and DVI have similar radiative transfer features and are strongly linearly correlated with

701   each other, while NDVI behaves differently as a ratio-based VI and is more impacted by soil

702   background. NIRv, EVI, EVI2 and DVI can reproduce the results of each other in most cases

703   because of their similarity.

704   Finally, we strongly recommend that future studies using VIs should be conducted with clear

705   focus on interpretation of VIs, and using more than one *in-situ* dataset for verification when

706   possible, to render greater confidence in their findings and conclusions. It would also be important

707   to provide a detailed documentation of the key processing steps mentioned above to facilitate the

708   interpretation and reproducibility of VI-based results. Ideally, the programming code should also

709   be provided or made available when requested, and where feasible, the final VI dataset should be

710   stored in a publicly accessible repository or cloud storage such as Google Earth Engine for ease of

711   access [181]. In particular, the documentation should include relevant information on the application

712   of QA/QC levels as well as any other processing steps such as spatio-temporal aggregation,

713   additional quality and outlier filtering or other corrections applied to the original data. Providing

714   such detailed technical information on VI products might be a promising strategy as then the

715   documentation would be straightforward to find and also citable via a doi linked to a given dataset

716   that is available for the user community. The technical review and recommendations presented

717   here are intended to further advance the use of VIs in scientific studies and reduce any confusion

718   and inconsistencies due to their improper use, considering the continued record length of existing

719   capabilities, such as MODIS and VIIRS instruments, and emerging new ones, such as HiSUI,

720   PRISMA and EnMap.

721   **References**

722   1   Bannari, A., Morin, D., Bonn, F. & Huete, A. A review of vegetation indices.
723   *Remote sensing reviews* **13**, 95-120 (1995).
724   2   Gao, X., Huete, A. R., Ni, W. & Miura, T. Optical–biophysical relationships of
725   vegetation spectra without background contamination. *Remote sensing of*
726   *environment* **74**, 609-620 (2000).
727   3   Huete, A. R. A soil-adjusted vegetation index (SAVI). *Remote sensing of*
728   *environment* **25**, 295-309 (1988).
729   4   Badgley, G., Field, C. B. & Berry, J. A. Canopy near-infrared reflectance and
730   terrestrial photosynthesis. *Science Advances* **3**, e1602244 (2017).
731   5   Gamon, J. A. *et al.* A remotely sensed pigment index reveals photosynthetic
732   phenology in evergreen conifers. *Proceedings of the National Academy of*
733   *Sciences* **113**, 13087-13092 (2016).
734   6   Joiner, J. *et al.* Estimation of terrestrial global gross primary production (GPP) with
735   satellite data-driven models and eddy covariance flux data. *Remote Sensing* **10**,
736   1346 (2018).

737 7   Piao, S. *et al.* Characteristics, drivers and feedbacks of global greening. *Nature Reviews Earth & Environment* **1**, 14-27 (2020).
738
739 8   Tian, F. *et al.* Evaluating temporal consistency of long-term global NDVI datasets for trend analysis. *Remote Sensing of Environment* **163**, 326-340 (2015).
740
741 9   Fan, X. & Liu, Y. A global study of NDVI difference among moderate-resolution satellite sensors. *ISPRS Journal of Photogrammetry and Remote Sensing* **121**, 177-191 (2016).
742
743
744 10 AghaKouchak, A. *et al.* Remote sensing of drought: Progress, challenges and opportunities. *Reviews of Geophysics* **53**, 452-480 (2015).
745
746 11 Anyamba, A. & Tucker, C. J. Historical perspective of AVHRR NDVI and vegetation drought monitoring. *Remote sensing of drought: Innovative monitoring approaches* **23**, 20 (2012).
747
748
749 12 Veraverbeke, S. *et al.* Hyperspectral remote sensing of fire: State-of-the-art and future perspectives. *Remote Sensing of Environment* **216**, 105-121 (2018).
750
751 13 Houborg, R., Fisher, J. B. & Skidmore, A. K. Advances in remote sensing of vegetation function and traits. *International Journal of Applied Earth Observation and Geoinformation* **43**, 1-6 (2015).
752
753
754 14 Tucker, C. J. Red and photographic infrared linear combinations for monitoring vegetation. *Remote Sensing of Environment* **8**, 127-150, doi:http://dx.doi.org/10.1016/0034-4257(79)90013-0 (1979).
755
756
757 15 Rouse, J. W., Haas, R. H., Schell, J. A. & Deering, D. W. Monitoring vegetation systems in the Great Plains with ERTS. *NASA special publication* **351**, 309 (1974).
758
759 16 Rouse, J. W., Haas, R. H., Schell, J. A., Deering, D. W. & Harlan, J. C. Monitoring the vernal advancement and retrogradation (green wave effect) of natural vegetation. *NASA/GSFC Type III Final Report, Greenbelt, Md* **371** (1974).
760
761
762 17 Gutman, G., Skakun, S. & Gitelson, A. Revisiting the use of red and near-infrared reflectances in vegetation studies and numerical climate models. *Science of Remote Sensing* **4**, 100025 (2021).
763
764
765 18 Jackson, R. D. & Huete, A. R. Interpreting vegetation indices. *Preventive veterinary medicine* **11**, 185-200 (1991).
766
767 19 Richardson, A. J. & Wiegand, C. Distinguishing vegetation from soil background information. *Photogrammetric engineering and remote sensing* **43**, 1541-1552 (1977).
768
769
770 20 Baret, F., Guyot, G. & Major, D. in *12th Canadian Symposium on Remote Sensing Geoscience and Remote Sensing Symposium.* 1355-1358 (IEEE).
771
772 21 Qi, J., Chehbouni, A., Huete, A. R., Kerr, Y. H. & Sorooshian, S. A modified soil adjusted vegetation index. *Remote sensing of environment* **48**, 119-126 (1994).
773
774 22 Chen, J. M. Evaluation of vegetation indices and a modified simple ratio for boreal applications. *Canadian Journal of Remote Sensing* **22**, 229-242 (1996).
775
776 23 Brown, L., Chen, J. M., Leblanc, S. G. & Cihlar, J. A shortwave infrared modification to the simple ratio for LAI retrieval in boreal forests: An image and model analysis. *Remote sensing of environment* **71**, 16-25 (2000).
777
778
779 24 Pinty, B. & Verstraete, M. GEMI: a non-linear index to monitor global vegetation from satellites. *Vegetatio* **101**, 15-20 (1992).
780
781 25 Huete, A. *et al.* Overview of the radiometric and biophysical performance of the MODIS vegetation indices. *Remote Sensing of Environment* **83**, 195-213, doi:http://dx.doi.org/10.1016/S0034-4257(02)00096-2 (2002).
782
783
784 26 Kaufman, Y. J. & Tanre, D. Atmospherically resistant vegetation index (ARVI) for EOS-MODIS. *IEEE transactions on Geoscience and Remote Sensing* **30**, 261-270 (1992).
785
786
787 27 Jiang, Z., Huete, A. R., Didan, K. & Miura, T. Development of a two-band enhanced vegetation index without a blue band. *Remote sensing of Environment* **112**, 3833-3845 (2008).
788
789

790 28 Jin, H. & Eklundh, L. A physically based vegetation index for improved monitoring
791   of plant phenology. *Remote Sensing of Environment* **152**, 512-525,
792   doi:10.1016/j.rse.2014.07.010 (2014).
793 29 Yang, P., van der Tol, C., Campbell, P. K. & Middleton, E. M. Fluorescence
794   Correction Vegetation Index (FCVI): A physically based reflectance index to
795   separate physiological and non-physiological information in far-red sun-induced
796   chlorophyll fluorescence. *Remote sensing of environment* **240**, 111676 (2020).
797 30 Badgley, G., Anderegg, L. D., Berry, J. A. & Field, C. B. Terrestrial gross primary
798   production: Using NIRV to scale from site to globe. *Global change biology* **25**,
799   3731-3740 (2019).
800 31 Camps-Valls, G. *et al.* A unified vegetation index for quantifying the terrestrial
801   biosphere. *Science Advances* **7**, eabc7447 (2021).
802 32 Roberts, D. A., Roth, K. L. & Perroy, R. L. 14 hyperspectral vegetation indices.
803   *Hyperspectral remote sensing of vegetation* **309** (2016).
804 33 Gitelson, A. A., Vina, A., Ciganda, V., Rundquist, D. C. & Arkebauer, T. J. Remote
805   estimation of canopy chlorophyll content in crops. *Geophysical Research Letters*
806   **32** (2005).
807 34 Gitelson, A. & Merzlyak, M. N. Spectral reflectance changes associated with
808   autumn senescence of Aesculus hippocastanum L. and Acer platanoides L. leaves.
809   Spectral features and relation to chlorophyll estimation. *Journal of plant physiology*
810   **143**, 286-292 (1994).
811 35 Dash, J. & Curran, P. The MERIS terrestrial chlorophyll index. *International
812   Journal of Remote Sensing* **25**, 5403-5413 (2004).
813 36 Penuelas, J., Baret, F. & Filella, I. Semi-empirical indices to assess
814   carotenoids/chlorophyll a ratio from leaf spectral reflectance. *Photosynthetica* **31**,
815   221-230 (1995).
816 37 Peñuelas, J., Gamon, J., Fredeen, A., Merino, J. & Field, C. Reflectance indices
817   associated with physiological changes in nitrogen-and water-limited sunflower
818   leaves. *Remote sensing of Environment* **48**, 135-146 (1994).
819 38 Merzlyak, M. N., Gitelson, A. A., Chivkunova, O. B. & Rakitin, V. Y. Non‐
820   destructive optical detection of pigment changes during leaf senescence and fruit
821   ripening. *Physiologia plantarum* **106**, 135-141 (1999).
822 39 Gitelson, A. A., Merzlyak, M. N. & Chivkunova, O. B. Optical properties and
823   nondestructive estimation of anthocyanin content in plant leaves. *Photochemistry
824   and photobiology* **74**, 38-45 (2001).
825 40 van den Berg, A. K. & Perkins, T. D. Nondestructive estimation of anthocyanin
826   content in autumn sugar maple leaves. *HortScience* **40**, 685-686 (2005).
827 41 Gamon, J. & Surfus, J. Assessing leaf pigment content and activity with a
828   reflectometer. *The New Phytologist* **143**, 105-117 (1999).
829 42 Gao, B.-C. NDWI—A normalized difference water index for remote sensing of
830   vegetation liquid water from space. *Remote sensing of environment* **58**, 257-266
831   (1996).
832 43 Xiao, X., Boles, S., Liu, J., Zhuang, D. & Liu, M. Characterization of forest types in
833   Northeastern China, using multi-temporal SPOT-4 VEGETATION sensor data.
834   *Remote Sensing of Environment* **82**, 335-348 (2002).
835 44 Xiao, X. *et al.* Satellite-based modeling of gross primary production in an
836   evergreen needleleaf forest. *Remote sensing of environment* **89**, 519-534 (2004).
837 45 Yilmaz, M. T., Hunt Jr, E. R. & Jackson, T. J. Remote sensing of vegetation water
838   content from equivalent water thickness using satellite imagery. *Remote Sensing
839   of Environment* **112**, 2514-2522 (2008).
840 46 Cheng, Y.-B., Ustin, S. L., Riaño, D. & Vanderbilt, V. C. Water content estimation
841   from hyperspectral images and MODIS indexes in Southeastern Arizona. *Remote
842   Sensing of Environment* **112**, 363-374 (2008).

843 47 Serrano, L., Penuelas, J. & Ustin, S. L. Remote sensing of nitrogen and lignin in
844 Mediterranean vegetation from AVIRIS data: Decomposing biochemical from
845 structural signals. *Remote sensing of Environment* **81**, 355-364 (2002).
846 48 Filella, I. *et al.* PRI assessment of long-term changes in carotenoids/chlorophyll
847 ratio and short-term changes in de-epoxidation state of the xanthophyll cycle.
848 *International Journal of Remote Sensing* **30**, 4443-4455 (2009).
849 49 Gamon, J., Penuelas, J. & Field, C. A narrow-waveband spectral index that tracks
850 diurnal changes in photosynthetic efficiency. *Remote Sensing of environment* **41**,
851 35-44 (1992).
852 50 Cheng, R. *et al.* Decomposing reflectance spectra to track gross primary
853 production in a subalpine evergreen forest. *Biogeosciences* **17**, 4523-4544 (2020).
854 51 Seyednasrollah, B. *et al.* Seasonal variation in the canopy color of temperate
855 evergreen conifer forests. *New Phytologist* **229**, 2586-2600 (2021).
856 52 Merton, R. in *Proceedings of the Seventh Annual JPL Airborne Earth Science*
857 *Workshop.* 12-16.
858 53 Naidu, R. A., Perry, E. M., Pierce, F. J. & Mekuria, T. The potential of spectral
859 reflectance technique for the detection of Grapevine leafroll-associated virus-3 in
860 two red-berried wine grape cultivars. *Computers and Electronics in Agriculture* **66**,
861 38-45 (2009).
862 54 Chen, Y. *et al.* Generation and evaluation of LAI and FPAR products from
863 Himawari-8 advanced Himawari imager (AHI) data. *Remote Sensing* **11**, 1517
864 (2019).
865 55 Zhu, Z. *et al.* Global Data Sets of Vegetation Leaf Area Index (LAI)3g and Fraction
866 of Photosynthetically Active Radiation (FPAR)3g Derived from Global Inventory
867 Modeling and Mapping Studies (GIMMS) Normalized Difference Vegetation Index
868 (NDVI3g) for the Period 1981 to 2011. *Remote Sensing* **5**, 927-948,
869 doi:10.3390/rs5020927 (2013).
870 56 Liu, Y., Liu, R. & Chen, J. M. Retrospective retrieval of long-term consistent global
871 leaf area index (1981–2011) from combined AVHRR and MODIS data. *Journal of*
872 *Geophysical Research* **117**, doi:10.1029/2012jg002084 (2012).
873 57 Croft, H. *et al.* The global distribution of leaf chlorophyll content. *Remote Sensing*
874 *of Environment* **236**, 111479 (2020).
875 58 Jiang, Z. *et al.* Analysis of NDVI and scaled difference vegetation index retrievals
876 of vegetation fraction. *Remote sensing of environment* **101**, 366-378 (2006).
877 59 Haboudane, D., Miller, J. R., Pattey, E., Zarco-Tejada, P. J. & Strachan, I. B.
878 Hyperspectral vegetation indices and novel algorithms for predicting green LAI of
879 crop canopies: Modeling and validation in the context of precision agriculture.
880 *Remote sensing of environment* **90**, 337-352 (2004).
881 60 Wu, C., Wang, L., Niu, Z., Gao, S. & Wu, M. Nondestructive estimation of canopy
882 chlorophyll content using Hyperion and Landsat/TM images. *International Journal*
883 *of Remote Sensing* **31**, 2159-2167 (2010).
884 61 Wang, R. & Gamon, J. A. Remote sensing of terrestrial plant biodiversity. *Remote*
885 *Sensing of Environment* **231**, 111218 (2019).
886 62 Ustin, S. L. & Gamon, J. A. Remote sensing of plant functional types. *New*
887 *Phytologist* **186**, 795-816 (2010).
888 63 Hilker, T. *et al.* Vegetation dynamics and rainfall sensitivity of the Amazon.
889 *Proceedings of the National Academy of Sciences* **111**, 16041-16046 (2014).
890 64 Zhang, Y., Commane, R., Zhou, S., Williams, A. P. & Gentine, P. Light limitation
891 regulates the response of autumn terrestrial carbon uptake to warming. *Nature*
892 *Climate Change* **10**, 739-743 (2020).
893 65 Weber, M. *et al.* Exploring the use of DSCOVR/EPIC satellite observations to
894 monitor vegetation phenology. *Remote Sensing* **12**, 2384 (2020).
895 66 Wang, S., Zhang, Y., Ju, W., Qiu, B. & Zhang, Z. Tracking the seasonal and inter-
896 annual variations of global gross primary production during last four decades using

897   satellite near-infrared reflectance data. *Science of the Total Environment* **755**,
898   142569 (2021).

899   67   Tian, F. *et al.* Calibrating vegetation phenology from Sentinel-2 using eddy
900   covariance, PhenoCam, and PEP725 networks across Europe. *Remote Sensing*
901   *of Environment* **260**, 112456 (2021).

902   68   Yin, G., Verger, A., Filella, I., Descals, A. & Peñuelas, J. Divergent estimates of
903   forest photosynthetic phenology using structural and physiological vegetation
904   indices. *Geophysical Research Letters* **47**, e2020GL089167 (2020).

905   69   Qin, Y. *et al.* Carbon loss from forest degradation exceeds that from deforestation
906   in the Brazilian Amazon. *Nature Climate Change* **11**, 442-448 (2021).

907   70   Samanta, A. *et al.* Amazon forests did not green‐up during the 2005 drought.
908   *Geophysical research letters* **37** (2010).

909   71   Shi, Y., Huang, W., Luo, J., Huang, L. & Zhou, X. Detection and discrimination of
910   pests and diseases in winter wheat based on spectral indices and kernel
911   discriminant analysis. *Computers and Electronics in Agriculture* **141**, 171-180
912   (2017).

913   72   Zhang, Z., Liu, M., Liu, X. & Zhou, G. A new vegetation index based on
914   multitemporal Sentinel-2 images for discriminating heavy metal stress levels in rice.
915   *Sensors* **18**, 2172 (2018).

916   73   Yengoh, G. T., Dent, D., Olsson, L., Tengberg, A. E. & Tucker III, C. J. *Use of the*
917   *Normalized Difference Vegetation Index (NDVI) to assess Land degradation at*
918   *multiple scales: current status, future trends, and practical considerations*.
919   (Springer, 2015).

920   74   Potter, C. S. *et al.* Terrestrial ecosystem production: a process model based on
921   global satellite and surface data. *Global Biogeochemical Cycles* **7**, 811-841 (1993).

922   75   Running, S. W. *et al.* A continuous satellite-derived measure of global terrestrial
923   primary production. *Bioscience* **54**, 547-560 (2004).

924   76   Yuan, W. *et al.* Deriving a light use efficiency model from eddy covariance flux
925   data for predicting daily gross primary production across biomes. *Agricultural and*
926   *Forest Meteorology* **143**, 189-207 (2007).

927   77   Chen, M. *et al.* Quantification of terrestrial ecosystem carbon dynamics in the
928   conterminous United States combining a process-based biogeochemical model
929   and MODIS and AmeriFlux data. *Biogeosciences* **8**, 2665-2688 (2011).

930   78   Xiao, J. *et al.* A continuous measure of gross primary production for the
931   conterminous United States derived from MODIS and AmeriFlux data. *Remote*
932   *sensing of environment* **114**, 576-591 (2010).

933   79   Jiang, C., Guan, K., Wu, G., Peng, B. & Wang, S. A daily, 250 m, and real-time
934   gross primary productivity product (2000–present) covering the Contiguous United
935   States. *Earth Syst. Sci. Data Discuss.* **2020**, 1-28 (2020).

936   80   Schubert, P. *et al.* Modeling GPP in the Nordic forest landscape with MODIS time
937   series data—Comparison with the MODIS GPP product. *Remote Sensing of*
938   *Environment* **126**, 136-147 (2012).

939   81   Zeng, Y. *et al.* A practical approach for estimating the escape ratio of near-infrared
940   solar-induced chlorophyll fluorescence. *Remote Sensing of Environment* **232**,
941   111209 (2019).

942   82   Baldocchi, D. D. *et al.* Outgoing Near Infrared Radiation from Vegetation Scales
943   with Canopy Photosynthesis Across a Spectrum of Function, Structure,
944   Physiological Capacity and Weather. *Journal of Geophysical Research:*
945   *Biogeosciences*, e2019JG005534 (2020).

946   83   Dechant, B. *et al.* Canopy structure explains the relationship between
947   photosynthesis and sun-induced chlorophyll fluorescence in crops. *Remote*
948   *Sensing of Environment* **241**, 111733 (2020).

949   84   Rahman, A. F., Gamon, J. A., Fuentes, D. A., Roberts, D. A. & Prentiss, D.
950   Modeling spatially distributed ecosystem flux of boreal forest using hyperspectral

951   indices from AVIRIS imagery. *Journal of Geophysical Research: Atmospheres* **106**,
952   33579-33591 (2001).
953 85 Wang, S. *et al.* Recent global decline of CO2 fertilization effects on vegetation
954   photosynthesis. *Science* **370**, 1295-1300 (2020).
955 86 Zhu, Z. *et al.* Comment on "Recent global decline of CO2 fertilization effects on
956   vegetation photosynthesis". *Science* **373**, eabg5673 (2021).
957 87 Huang, M. *et al.* Air temperature optima of vegetation productivity across global
958   biomes. *Nature ecology & evolution* **3**, 772-779 (2019).
959 88 Doughty, R. *et al.* Small anomalies in dry-season greenness and chlorophyll
960   fluorescence for Amazon moist tropical forests during El Niño and La Niña.
961   *Remote Sensing of Environment* **253**, 112196 (2021).
962 89 Wigneron, J.-P. *et al.* Tropical forests did not recover from the strong 2015–2016
963   El Niño event. *Science advances* **6**, eaay4603 (2020).
964 90 Huang, N. *et al.* Spatial and temporal variations in global soil respiration and their
965   relationships with climate and land cover. *Science advances* **6**, eabb8508 (2020).
966 91 Huang, N., He, J.-S. & Niu, Z. Estimating the spatial pattern of soil respiration in
967   Tibetan alpine grasslands using Landsat TM images and MODIS data. *Ecological
968   Indicators* **26**, 117-125 (2013).
969 92 Neale, C. M., Gonzalez‐Dugo, M. P., Serrano‐Perez, A., Campos, I. & Mateos,
970   L. Cotton canopy reflectance under variable solar zenith angles: Implications of
971   use in evapotranspiration models. *Hydrological Processes* **35**, e14162 (2021).
972 93 Chen, J. M. & Liu, J. Evolution of evapotranspiration models using thermal and
973   shortwave remote sensing data. *Remote Sensing of Environment* **237**, 111594
974   (2020).
975 94 Glenn, E. P., Huete, A. R., Nagler, P. L. & Nelson, S. G. Relationship between
976   remotely-sensed vegetation indices, canopy attributes and plant physiological
977   processes: What vegetation indices can and cannot tell us about the landscape.
978   *Sensors* **8**, 2136-2160 (2008).
979 95 Cui, Y., Jia, L. & Fan, W. Estimation of actual evapotranspiration and its
980   components in an irrigated area by integrating the Shuttleworth-Wallace and
981   surface temperature-vegetation index schemes using the particle swarm
982   optimization algorithm. *Agricultural and Forest Meteorology* **307**, 108488 (2021).
983 96 Glenn, E. P., Neale, C. M., Hunsaker, D. J. & Nagler, P. L. Vegetation index‐
984   based crop coefficients to estimate evapotranspiration by remote sensing in
985   agricultural and natural ecosystems. *Hydrological Processes* **25**, 4050-4062
986   (2011).
987 97 French, A. N. *et al.* Satellite-based NDVI crop coefficients and evapotranspiration
988   with eddy covariance validation for multiple durum wheat fields in the US
989   Southwest. *Agricultural Water Management* **239**, 106266 (2020).
990 98 Fensholt, R. & Proud, S. R. Evaluation of earth observation based global long term
991   vegetation trends—Comparing GIMMS and MODIS global NDVI time series.
992   *Remote sensing of Environment* **119**, 131-147 (2012).
993 99 Trishchenko, A. P., Cihlar, J. & Li, Z. Effects of spectral response function on
994   surface reflectance and NDVI measured with moderate resolution satellite sensors.
995   *Remote Sensing of Environment* **81**, 1-18 (2002).
996 100 Ustin, S. L. & Middleton, E. M. Current and near-term advances in Earth
997   observation for ecological applications. *Ecological processes* **10**, 1-57 (2021).
998 101 Wang, D. *et al.* Impact of sensor degradation on the MODIS NDVI time series.
999   *Remote Sensing of Environment* **119**, 55-61 (2012).
1000 102 Zhang, Y., Song, C., Band, L. E., Sun, G. & Li, J. Reanalysis of global terrestrial
1001   vegetation trends from MODIS products: Browning or greening? *Remote Sensing
1002   of Environment* **191**, 145-155 (2017).

103   Bhatt, R. *et al.* A consistent AVHRR visible calibration record based on multiple methods applicable for the NOAA degrading orbits. Part I: Methodology. *Journal of Atmospheric and Oceanic Technology* **33**, 2499-2515 (2016).

104   Frankenberg, C., Yin, Y., Byrne, B., He, L. & Gentine, P. COMMENT ON "RECENT GLOBAL DECLINE OF CO2 FERTILIZATION EFFECTS ON VEGETATION PHOTOSYNTHESIS". *Science* **373**, eabg2947, doi:10.1126/science.abg2947 (2021).

105   Los, S. O. Estimation of the ratio of sensor degradation between NOAA AVHRR channels 1 and 2 from monthly NDVI composites. *IEEE Transactions on Geoscience and Remote Sensing* **36**, 206-213 (1998).

106   Jiang, C. *et al.* Inconsistencies of interannual variability and trends in long‐term satellite leaf area index products. *Global Change Biology* **23**, 4133-4146 (2017).

107   de Beurs, K. M. & Henebry, G. M. Trend analysis of the Pathfinder AVHRR Land (PAL) NDVI data for the deserts of Central Asia. *IEEE Geoscience and Remote Sensing Letters* **1**, 282-286 (2004).

108   Wang, Z. *et al.* Large discrepancies of global greening: Indication of multi-source remote sensing data. *Global Ecology and Conservation*, e02016 (2022).

109   Miura, T., Huete, A. R. & Yoshioka, H. Evaluation of sensor calibration uncertainties on vegetation indices for MODIS. *Geoscience and Remote Sensing, IEEE Transactions on* **38**, 1399-1409 (2000).

110   Lyapustin, A. *et al.* Scientific impact of MODIS C5 calibration degradation and C6+ improvements. *Atmospheric Measurement Techniques* **7**, 4353-4365 (2014).

111   Buchhorn, M., Raynolds, M. K. & Walker, D. A. Influence of BRDF on NDVI and biomass estimations of Alaska Arctic tundra. *Environmental Research Letters* **11**, 125002 (2016).

112   Morton, D. C. *et al.* Amazon forests maintain consistent canopy structure and greenness during the dry season. *Nature* **506**, 221-224, doi:10.1038/nature13006 (2014).

113   Fensholt, R., Sandholt, I., Proud, S. R., Stisen, S. & Rasmussen, M. O. Assessment of MODIS sun-sensor geometry variations effect on observed NDVI using MSG SEVIRI geostationary data. *International Journal of Remote Sensing* **31**, 6163-6187 (2010).

114   Saleska, S. R. *et al.* Dry-season greening of Amazon forests. *Nature* **531**, E4-E5 (2016).

115   Lyapustin, A. I. *et al.* Multi-angle implementation of atmospheric correction for MODIS (MAIAC): 3. Atmospheric correction. *Remote Sensing of Environment* **127**, 385-393 (2012).

116   Norris, J. R. & Walker, J. J. Solar and sensor geometry, not vegetation response, drive satellite NDVI phenology in widespread ecosystems of the western United States. *Remote Sensing of Environment* **249**, 112013 (2020).

117   Roy, D. P. *et al.* A general method to normalize Landsat reflectance data to nadir BRDF adjusted reflectance. *Remote Sensing of Environment* **176**, 255-271 (2016).

118   Schaaf, C. B. *et al.* First operational BRDF, albedo nadir reflectance products from MODIS. *Remote sensing of Environment* **83**, 135-148 (2002).

119   Didan, K., Munoz, A. B., Solano, R. & Huete, A. MODIS vegetation index user's guide (MOD13 series). *University of Arizona: Vegetation Index and Phenology Lab* (2015).

120   Wang, Z., Schaaf, C. B., Sun, Q., Shuai, Y. & Román, M. O. Capturing rapid land surface dynamics with Collection V006 MODIS BRDF/NBAR/Albedo (MCD43) products. *Remote sensing of environment* **207**, 50-64 (2018).

121   Saleska, S. R., Didan, K., Huete, A. R. & Da Rocha, H. R. Amazon forests green-up during 2005 drought. *Science* **318**, 612-612 (2007).

1055 122 Vargas, M., Miura, T., Shabanov, N. & Kato, A. An initial assessment of Suomi
1056   NPP VIIRS vegetation index EDR. *Journal of Geophysical Research:*
1057   *Atmospheres* **118**, 12,301-312,316 (2013).
1058 123 Kobayashi, H. & Dye, D. G. Atmospheric conditions for monitoring the long-term
1059   vegetation dynamics in the Amazon using normalized difference vegetation index.
1060   *Remote Sensing of Environment* **97**, 519-525 (2005).
1061 124 Jiang, C. & Fang, H. GSV: a general model for hyperspectral soil reflectance
1062   simulation. *International Journal of Applied Earth Observation and Geoinformation*
1063   **83**, 101932 (2019).
1064 125 Verrelst, J., Schaepman, M. E., Malenovský, Z. & Clevers, J. G. Effects of woody
1065   elements on simulated canopy reflectance: Implications for forest chlorophyll
1066   content retrieval. *Remote Sensing of Environment* **114**, 647-656 (2010).
1067 126 Huete, A. & Tucker, C. Investigation of soil influences in AVHRR red and near-
1068   infrared vegetation index imagery. *International journal of remote sensing* **12**,
1069   1223-1242 (1991).
1070 127 Farrar, T., Nicholson, S. & Lare, A. The influence of soil type on the relationships
1071   between NDVI, rainfall, and soil moisture in semiarid Botswana. II. NDVI response
1072   to soil oisture. *Remote sensing of Environment* **50**, 121-133 (1994).
1073 128 Huete, A. & Warrick, A. Assessment of vegetation and soil water regimes in partial
1074   canopies with optical remotely sensed data. *Remote Sensing of Environment* **32**,
1075   155-167 (1990).
1076 129 Wang, C. *et al.* A snow-free vegetation index for improved monitoring of vegetation
1077   spring green-up date in deciduous ecosystems. *Remote sensing of environment*
1078   **196**, 1-12 (2017).
1079 130 Myers-Smith, I. H. *et al.* Complexity revealed in the greening of the Arctic. *Nature*
1080   *Climate Change* **10**, 106-117 (2020).
1081 131 Shen, M. *et al.* No evidence of continuously advanced green-up dates in the
1082   Tibetan Plateau over the last decade. *Proceedings of the National Academy of*
1083   *Sciences* **110**, E2329-E2329 (2013).
1084 132 Grover, V. I., Borsdorf, A., Breuste, J., Tiwari, P. C. & Frangetto, F. W. *Impact of*
1085   *global changes on mountains: responses and adaptation.* (CRC Press, 2014).
1086 133 Hao, D. *et al.* Modeling anisotropic reflectance over composite sloping terrain.
1087   *IEEE Transactions on Geoscience and Remote Sensing* **56**, 3903-3923 (2018).
1088 134 Matsushita, B., Yang, W., Chen, J., Onda, Y. & Qiu, G. Sensitivity of the enhanced
1089   vegetation index (EVI) and normalized difference vegetation index (NDVI) to
1090   topographic effects: a case study in high-density cypress forest. *Sensors* **7**, 2636-
1091   2651 (2007).
1092 135 Wen, J. *et al.* Characterizing land surface anisotropic reflectance over rugged
1093   terrain: A review of concepts and recent developments. *Remote Sensing* **10**, 370
1094   (2018).
1095 136 Friedl, M. A., Davis, F. W., Michaelsen, J. & Moritz, M. Scaling and uncertainty in
1096   the relationship between the NDVI and land surface biophysical variables: An
1097   analysis using a scene simulation model and data from FIFE. *Remote Sensing of*
1098   *Environment* **54**, 233-246 (1995).
1099 137 Tan, B. *et al.* The impact of gridding artifacts on the local spatial properties of
1100   MODIS data: Implications for validation, compositing, and band-to-band
1101   registration across resolutions. *Remote Sensing of Environment* **105**, 98-114
1102   (2006).
1103 138 Wolfe, R. E. *et al.* Achieving sub-pixel geolocation accuracy in support of MODIS
1104   land science. *Remote Sensing of Environment* **83**, 31-49 (2002).
1105 139 Ferreira, M. P. *et al.* Retrieving structural and chemical properties of individual tree
1106   crowns in a highly diverse tropical forest with 3D radiative transfer modeling and
1107   imaging spectroscopy. *Remote Sensing of Environment* **211**, 276-291 (2018).

1108   140   Huete, A. R. *et al.* Amazon rainforests green‐up with sunlight in dry season.
1109   *Geophysical research letters* **33** (2006).
1110   141   Herrmann, S. M. & Tappan, G. G. Vegetation impoverishment despite greening: A
1111   case study from central Senegal. *Journal of Arid Environments* **90**, 55-66 (2013).
1112   142   Wang, X. *et al.* No consistent evidence for advancing or delaying trends in spring
1113   phenology on the Tibetan Plateau. *Journal of Geophysical Research:*
1114   *Biogeosciences* **122**, 3288-3305 (2017).
1115   143   Donnelly, A., Yu, R. & Liu, L. Comparing in situ spring phenology and satellite-
1116   derived start of season at rural and urban sites in Ireland. *International Journal of*
1117   *Remote Sensing* **42**, 7821-7841 (2021).
1118   144   Templ, B. *et al.* Pan European Phenological database (PEP725): a single point of
1119   access for European data. *International journal of biometeorology* **62**, 1109-1113
1120   (2018).
1121   145   Fu, Y. H. *et al.* Declining global warming effects on the phenology of spring leaf
1122   unfolding. *Nature* **526**, 104-107 (2015).
1123   146   Chen, X. & Yang, Y. Observed earlier start of the growing season from middle to
1124   high latitudes across the Northern Hemisphere snow-covered landmass for the
1125   period 2001–2014. *Environmental Research Letters* **15**, 034042 (2020).
1126   147   Alatorre, L. C. *et al.* Temporal changes of NDVI for qualitative environmental
1127   assessment of mangroves: shrimp farming impact on the health decline of the arid
1128   mangroves in the Gulf of California (1990–2010). *Journal of Arid Environments*
1129   **125**, 98-109 (2016).
1130   148   Jacquemoud, S. & Baret, F. PROSPECT: A model of leaf optical properties
1131   spectra. *Remote sensing of environment* **34**, 75-91 (1990).
1132   149   Wu, S. *et al.* Quantifying leaf optical properties with spectral invariants theory.
1133   *Remote Sensing of Environment* **253**, 112131 (2021).
1134   150   Wang, Z. *et al.* Mapping foliar functional traits and their uncertainties across three
1135   years in a grassland experiment. *Remote Sensing of Environment* **221**, 405-416
1136   (2019).
1137   151   Van Leeuwen, W. & Huete, A. Effects of standing litter on the biophysical
1138   interpretation of plant canopies with spectral indices. *Remote sensing of*
1139   *Environment* **55**, 123-138 (1996).
1140   152   Dechant, B. *et al.* NIRvP: A robust structural proxy for sun-induced chlorophyll
1141   fluorescence and photosynthesis across scales. *Remote Sensing of Environment*
1142   **268**, 112763 (2022).
1143   153   Zeng, Y. *et al.* Estimating near-infrared reflectance of vegetation from
1144   hyperspectral data. *Remote Sensing of Environment* **267**, 112723 (2021).
1145   154   Hantson, S. & Chuvieco, E. Evaluation of different topographic correction methods
1146   for Landsat imagery. *International Journal of Applied Earth Observation and*
1147   *Geoinformation* **13**, 691-700 (2011).
1148   155   Zhang, H. K. *et al.* Characterization of Sentinel-2A and Landsat-8 top of
1149   atmosphere, surface, and nadir BRDF adjusted reflectance and NDVI differences.
1150   *Remote sensing of environment* **215**, 482-494 (2018).
1151   156   Gao, F., Masek, J., Schwaller, M. & Hall, F. On the blending of the Landsat and
1152   MODIS surface reflectance: Predicting daily Landsat surface reflectance. *IEEE*
1153   *Transactions on Geoscience and Remote sensing* **44**, 2207-2218 (2006).
1154   157   Zhu, X. *et al.* A flexible spatiotemporal method for fusing satellite images with
1155   different resolutions. *Remote Sensing of Environment* **172**, 165-177 (2016).
1156   158   Luo, Y., Guan, K. & Peng, J. STAIR: A generic and fully-automated method to fuse
1157   multiple sources of optical satellite data to generate a high-resolution, daily and
1158   cloud-/gap-free surface reflectance product. *Remote Sensing of Environment* **214**,
1159   87-99 (2018).

1160 159 Houborg, R. & McCabe, M. F. Daily Retrieval of NDVI and LAI at 3 m Resolution
1161   via the Fusion of CubeSat, Landsat, and MODIS Data. *Remote Sensing* **10**, 890
1162   (2018).
1163 160 Kimm, H. *et al.* Deriving high-spatiotemporal-resolution leaf area index for
1164   agroecosystems in the US Corn Belt using Planet Labs CubeSat and STAIR
1165   fusion data. *Remote Sensing of Environment* **239**, 111615 (2020).
1166 161 Claverie, M. *et al.* The Harmonized Landsat and Sentinel-2 surface reflectance
1167   data set. *Remote Sensing of Environment* **219**, 145-161 (2018).
1168 162 Kong, J. *et al.* Evaluation of four image fusion NDVI products against in-situ
1169   spectral-measurements over a heterogeneous rice paddy landscape. *Agricultural*
1170   *and Forest Meteorology* **297**, 108255 (2021).
1171 163 Köhler, P. *et al.* Global retrievals of solar‐induced chlorophyll fluorescence with
1172   TROPOMI: First results and intersensor comparison to OCO‐2. *Geophysical*
1173   *Research Letters* **45**, 10,456-410,463 (2018).
1174 164 Sun, Y. *et al.* OCO-2 advances photosynthesis observation from space via solar-
1175   induced chlorophyll fluorescence. *Science* **358** (2017).
1176 165 Joiner, J., Yoshida, Y., Vasilkov, A. & Middleton, E. First observations of global
1177   and seasonal terrestrial chlorophyll fluorescence from space. *Biogeosciences* **8**,
1178   637-651 (2011).
1179 166 Frankenberg, C. *et al.* New global observations of the terrestrial carbon cycle from
1180   GOSAT: Patterns of plant fluorescence with gross primary productivity.
1181   *Geophysical Research Letters* **38** (2011).
1182 167 Qiu, B., Ge, J., Guo, W., Pitman, A. J. & Mu, M. Responses of Australian dryland
1183   vegetation to the 2019 heat wave at a subdaily scale. *Geophysical Research*
1184   *Letters* **47**, e2019GL086569 (2020).
1185 168 Magney, T. S. *et al.* Mechanistic evidence for tracking the seasonality of
1186   photosynthesis with solar-induced fluorescence. *Proceedings of the National*
1187   *Academy of Sciences* **116**, 11640-11645 (2019).
1188 169 Guanter, L. *et al.* Potential of the TROPOspheric Monitoring Instrument
1189   (TROPOMI) onboard the Sentinel-5 Precursor for the monitoring of terrestrial
1190   chlorophyll fluorescence. *Atmospheric Measurement Techniques* **8**, 1337-1352
1191   (2015).
1192 170 Knyazikhin, Y. *et al.* Hyperspectral remote sensing of foliar nitrogen content.
1193   *Proceedings of the National Academy of Sciences* **110**, E185-E192 (2013).
1194 171 Li, X. & Xiao, J. A global, 0.05-degree product of solar-induced chlorophyll
1195   fluorescence derived from OCO-2, MODIS, and reanalysis data. *Remote Sensing*
1196   **11**, 517 (2019).
1197 172 Zeng, Y. *et al.* Combining near-infrared radiance of vegetation and fluorescence
1198   spectroscopy to detect effects of abiotic changes and stresses. *Remote Sensing of*
1199   *Environment* **270**, 112856 (2022).
1200 173 Shi, J. *et al.* Microwave vegetation indices for short vegetation covers from satellite
1201   passive microwave sensor AMSR-E. *Remote sensing of environment* **112**, 4285-
1202   4300 (2008).
1203 174 Talebiesfandarani, S. *et al.* Microwave vegetation index from multi-angular
1204   observations and its application in vegetation properties retrieval: Theoretical
1205   modelling. *Remote Sensing* **11**, 730 (2019).
1206 175 Wigneron, J.-P. *et al.* SMOS-IC data record of soil moisture and L-VOD: Historical
1207   development, applications and perspectives. *Remote Sensing of Environment* **254**,
1208   112238 (2021).
1209 176 Zhang, Y., Zhou, S., Gentine, P. & Xiao, X. Can vegetation optical depth reflect
1210   changes in leaf water potential during soil moisture dry-down events? *Remote*
1211   *Sensing of Environment* **234**, 111451 (2019).
1212 177 Frappart, F. *et al.* Global monitoring of the vegetation dynamics from the
1213   Vegetation Optical Depth (VOD): A review. *Remote Sensing* **12**, 2915 (2020).

1214 178 Xiao, J., Fisher, J. B., Hashimoto, H., Ichii, K. & Parazoo, N. C. Emerging satellite
1215 observations for diurnal cycling of ecosystem processes. *Nature Plants*, 1-11
1216 (2021).
1217 179 Hashimoto, H. *et al.* New generation geostationary satellite observations support
1218 seasonality in greenness of the Amazon evergreen forests. *Nature
1219 communications* **12**, 1-11 (2021).
1220 180 Somkuti, P. *et al.* Solar-induced chlorophyll fluorescence from the Geostationary
1221 Carbon Cycle Observatory (GeoCarb): An extensive simulation study. *Remote
1222 Sensing of Environment* **263**, 112565 (2021).
1223 181 Gorelick, N. *et al.* Google Earth Engine: Planetary-scale geospatial analysis for
1224 everyone. *Remote sensing of Environment* **202**, 18-27 (2017).
1225 182 Baret, F. & Guyot, G. Potentials and limits of vegetation indices for LAI and APAR
1226 assessment. *Remote sensing of environment* **35**, 161-173 (1991).
1227 183 Broge, N. H. & Leblanc, E. Comparing prediction power and stability of broadband
1228 and hyperspectral vegetation indices for estimation of green leaf area index and
1229 canopy chlorophyll density. *Remote sensing of environment* **76**, 156-172 (2001).
1230 184 Nemani, R., Pierce, L., Running, S. & Band, L. Forest ecosystem processes at the
1231 watershed scale: sensitivity to remotely-sensed leaf area index estimates.
1232 *International journal of remote sensing* **14**, 2519-2534 (1993).
1233 185 Chamard, P. *et al.* Utilisation des bandes spectrales du vert et du rouge pour une
1234 meilleure évaluation des formations végétales actives. *Télédétection et
1235 cartographie*, 203-209 (1991).
1236 186 Gitelson, A. A. *et al.* Remote estimation of leaf area index and green leaf biomass
1237 in maize canopies. *Geophysical research letters* **30** (2003).
1238 187 Sripada, R. P., Heiniger, R. W., White, J. G. & Weisz, R. Aerial color infrared
1239 photography for determining late‐season nitrogen requirements in corn.
1240 *Agronomy Journal* **97**, 1443-1451 (2005).
1241 188 Gitelson, A. A., Kaufman, Y. J. & Merzlyak, M. N. Use of a green channel in
1242 remote sensing of global vegetation from EOS-MODIS. *Remote sensing of
1243 Environment* **58**, 289-298 (1996).
1244 189 Kim, M. S. *The Use of Narrow Spectral Bands for Improving Remote Sensing
1245 Estimations of Fractionally Absorbed Photosynthetically Active Radiation*, (1994).
1246 190 Daughtry, C. S., Walthall, C., Kim, M., De Colstoun, E. B. & McMurtrey Iii, J.
1247 Estimating corn leaf chlorophyll concentration from leaf and canopy reflectance.
1248 *Remote sensing of Environment* **74**, 229-239 (2000).
1249 191 Haboudane, D., Miller, J. R., Tremblay, N., Zarco-Tejada, P. J. & Dextraze, L.
1250 Integrated narrow-band vegetation indices for prediction of crop chlorophyll
1251 content for application to precision agriculture. *Remote sensing of environment* **81**,
1252 416-426 (2002).
1253 192 Blackburn, G. A. Spectral indices for estimating photosynthetic pigment
1254 concentrations: a test using senescent tree leaves. *International Journal of remote
1255 sensing* **19**, 657-675 (1998).
1256 193 Gitelson, A. A., Zur, Y., Chivkunova, O. B. & Merzlyak, M. N. Assessing carotenoid
1257 content in plant leaves with reflectance spectroscopy. *Photochemistry and
1258 photobiology* **75**, 272-281 (2002).
1259 194 Gitelson, A. A., Keydan, G. P. & Merzlyak, M. N. Three‐band model for
1260 noninvasive estimation of chlorophyll, carotenoids, and anthocyanin contents in
1261 higher plant leaves. *Geophysical research letters* **33** (2006).
1262 195 Steele, M. R., Gitelson, A. A., Rundquist, D. C. & Merzlyak, M. N. Nondestructive
1263 estimation of anthocyanin content in grapevine leaves. *American Journal of
1264 Enology and Viticulture* **60**, 87-92 (2009).
1265 196 Peñuelas, J., Pinol, J., Ogaya, R. & Filella, I. Estimation of plant water
1266 concentration by the reflectance water index WI (R900/R970). *International journal
1267 of remote sensing* **18**, 2869-2875 (1997).

1268   197   Daughtry, C. S. Discriminating crop residues from soil by shortwave infrared
1269   reflectance. *Agronomy Journal* **93**, 125-131 (2001).
1270   198   Daughtry, C. S., Hunt, E., Doraiswamy, P. & McMurtrey, J. Remote sensing the
1271   spatial distribution of crop residues. (2005).
1272   199   Richardson, A. D., Braswell, B. H., Hollinger, D. Y., Jenkins, J. P. & Ollinger, S. V.
1273   Near-surface remote sensing of spatial and temporal variation in canopy
1274   phenology. *Ecological Applications* **19**, 1417-1428, doi:10.1890/08-2022.1 (2009).
1275   200   Chen, B., Jin, Y. & Brown, P. An enhanced bloom index for quantifying floral
1276   phenology using multi-scale remote sensing observations. *ISPRS Journal of
1277   Photogrammetry and Remote Sensing* **156**, 108-120 (2019).
1278

Figures, tables and boxes
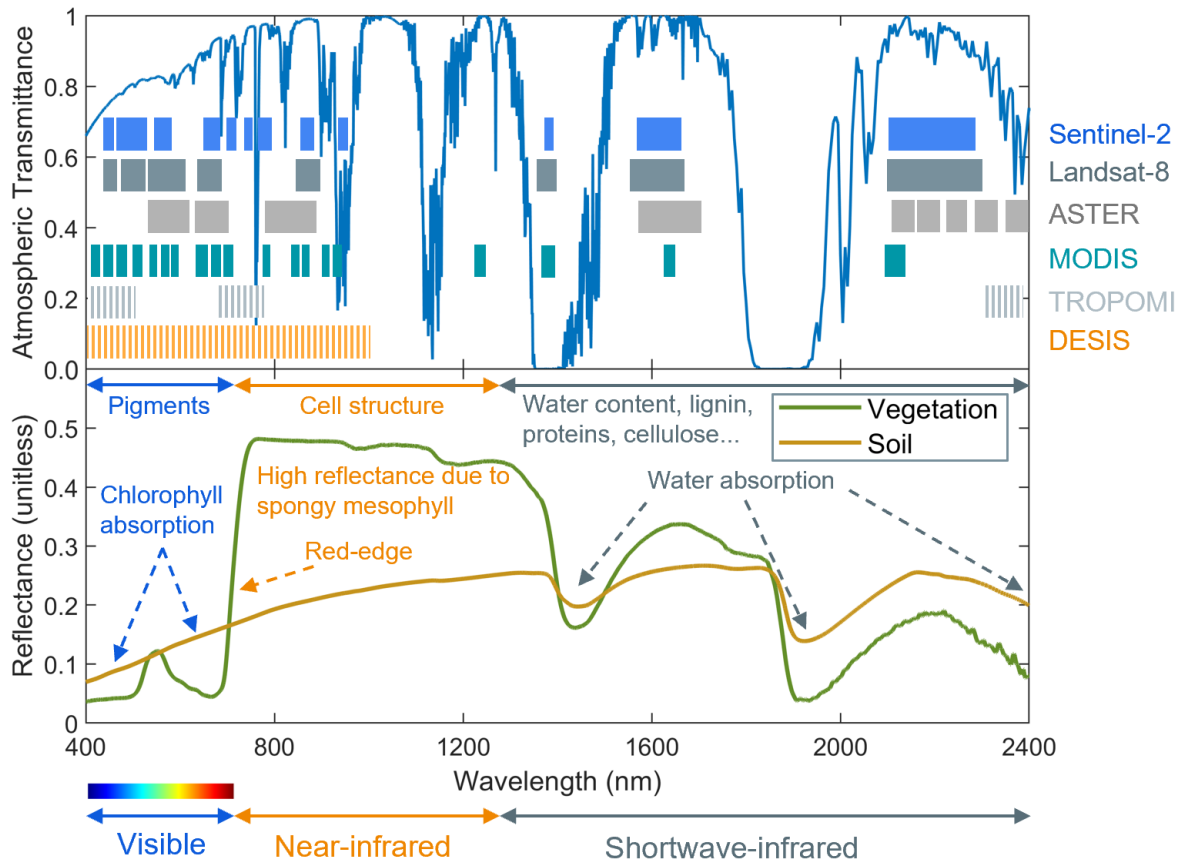
1281   **Fig. 1. The vegetation and soil spectrum across wavelengths to design vegetation indices**. The

1282   spectral response range in the atmospheric window of a few widely used satellites are also

1283   included[100]. The colored blocks and vertical lines in the top panel illustrate the spectral band range
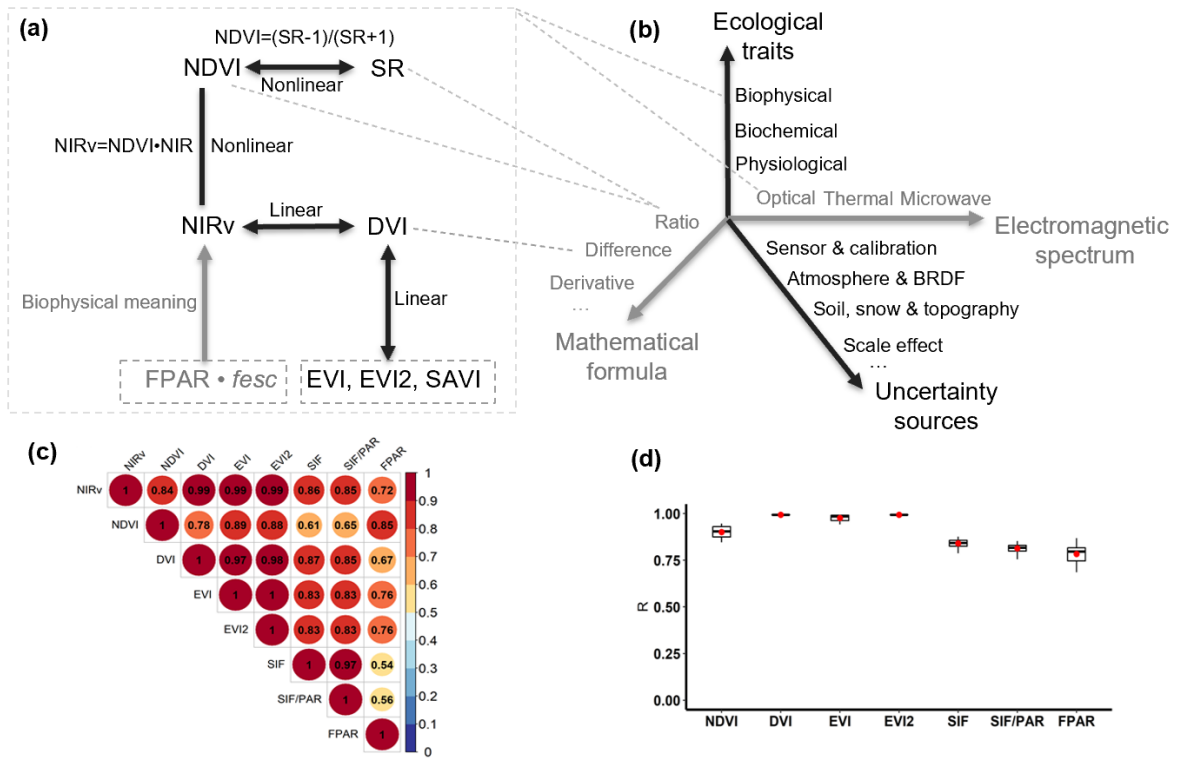
1284   or band pass for each satellite sensor.

1285
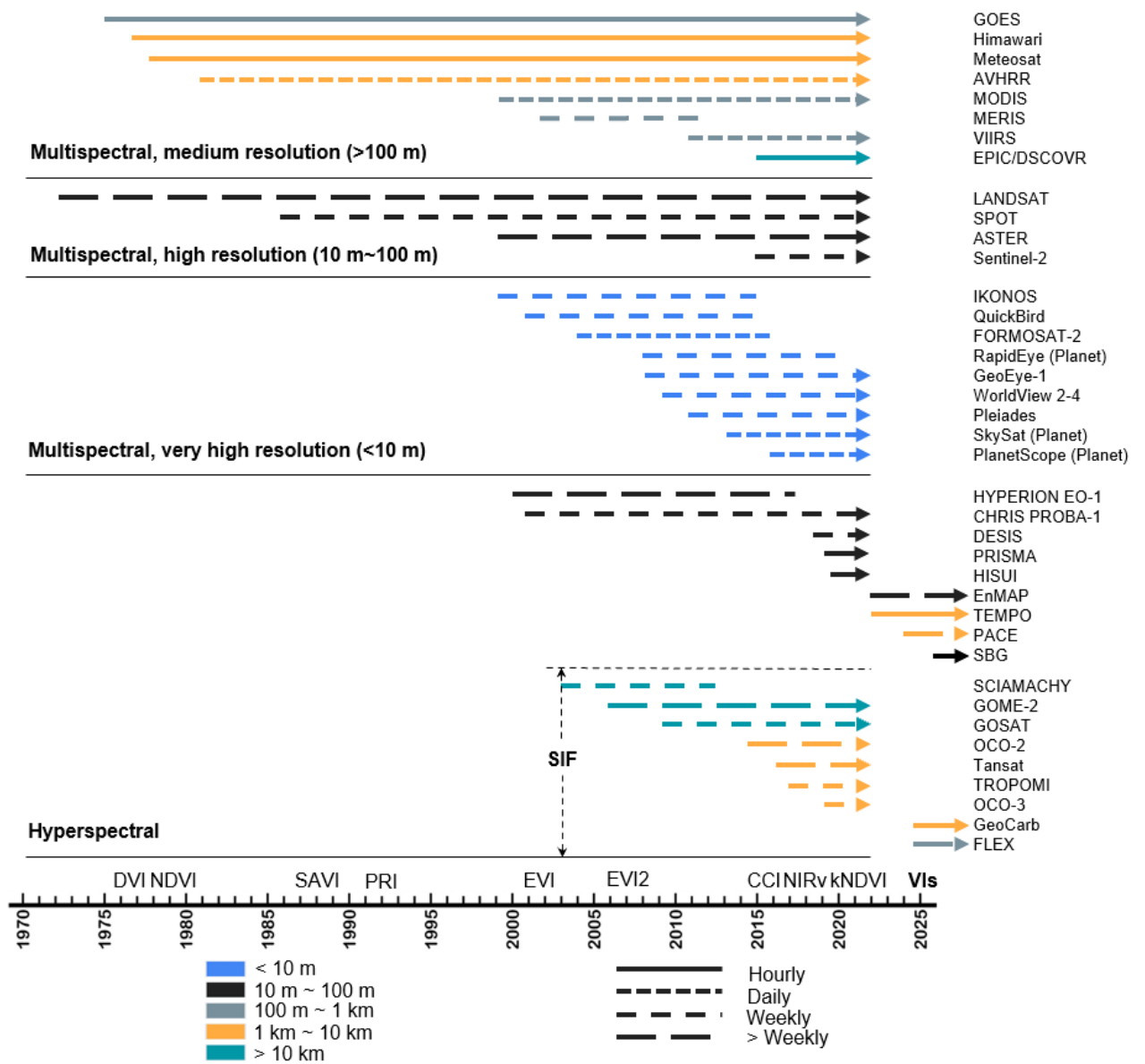
Fig. 2 The timeline of widely used satellites with the capability to derive VIs. The corresponding spatio-temporal resolutions are also included.

**Fig. 3 The taxonomy, physical meaning and similarity of VIs. a**| The biophysical interpretation and intrinsic linkage of several most widely used VIs in a variety of global-scale ecological studies. **b**| The taxonomy of VIs from four different dimensions: physics, mathematics, ecology and uncertainties. **c**| Global spatial correlations of monthly-averaged MODIS NIRv, DVI, EVI, EVI2, SIF, SIF/PAR (PAR-normalized SIF), NDVI and FPAR in August, 2018 and at 0.1° spatial resolution, considered as the peak growing month for most vegetation types. **d**| Global spatial correlations between MODIS NIRv and other remote sensing VIs during the 2018.03~2019.02 period since the origin of TROPOMI SIF, with the temporal resolution of 4 days and 0.1° spatial resolution. In the box plot, red circle refers to the mean value, boxes represent the interquartile ranges of the 25th (Q25) and 75th (Q75) percentiles, and whiskers cover the ranges of Q25 - 1.5·(Q75 - Q25) and Q75+1.5·(Q75 - Q25). The Rs among NIRv, DVI, EVI and EVI2 were greater than 0.95, while the R between NDVI and other VIs ranged from 0.78 to 0.89. NDVI has a relatively larger R with FPAR, but has a weaker linear correlation with SIF than the other VIs. In the spatial aggregation, the red, NIR and blue reflectance was firstly averagely aggregated to 0.1 degrees, and then the VIs were calculated.

1306
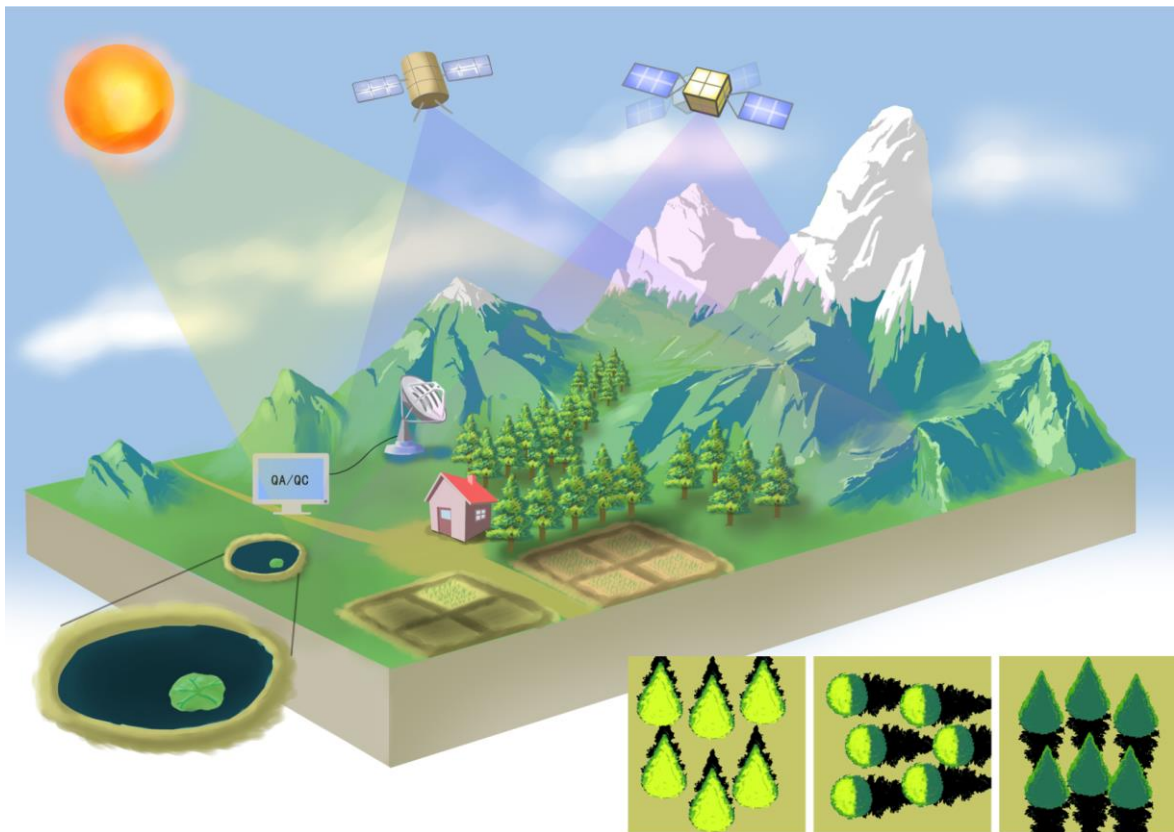
1307

1308 **Fig. 4 A sketch map of VIs from satellite observations.** Uncertainties come from different

1309 sensors and calibration, QA/QC flags and compositing algorithms, atmosphere and BRDF effects,

1310 soil/snow background and topography, and scale effects.

1311

1312

1313   **Table 1**: **The widely used optical vegetation indices, spectral ranges and references**

Spectral space	Name and references	Abbreviation	Equation and derivation	Primary applications, advantages and disadvantages
Red-NIR	Simple Ratio[14]	SR	NIR/Red	Structure; Simple but sensitive to the atmospheric correction of the red band
Red-NIR	Normalized Difference Vegetation Index[14-16]	NDVI	$(NIR - Red)/(NIR + Red)$ $= (SR - 1)/(SR + 1)$ $= 1 - 2/(SR + 1)$	Structure; Simple but sensitive to the soil background variations
Red-NIR	Modified Simple Ratio[22]	MSR	$\dfrac{NIR/Red - 1}{\sqrt{NIR/Red + 1}}$	Structure; More linear relationship with canopy structure parameters
Red-NIR	Difference Vegetation Index[19]	DVI	$NIR - Red$	Structure; Simple but sensitive to the BRDF effect
Red-NIR	Global Environment Monitoring Index[24]	GEMI	$\eta \cdot (1 - 0.25 \cdot \eta) - \dfrac{Red - 0.125}{1 - Red}$ η $= \dfrac{2 \cdot (NIR^2 - Red^2) + 1.5 \cdot NIR + 0.5 \cdot Red}{NIR + Red + 0.5}$	Structure; Reduce the atmospheric perturbation effects, while maintain the vegetation information
Red-NIR	Perpendicular Vegetation Index[19]	PVI	$\sqrt{(NIR_{soil} - NIR_{veg})^2 + (Red_{soil} - Red_{veg})^2}$	Structure; Minimize the soil background influence but need the slope and intercept of the soil line
Red-NIR	Soil Adjusted Vegetation Index[3]	SAVI	$(1 + L) \cdot (NIR - Red)/(NIR + Red + L)$	Structure; Minimize the soil background influence but sensitive to the BRDF effect

Red-NIR	Modified SAVI[21]	MSAVI	$(2 \cdot NIR + 1 - \sqrt{(2 \cdot NIR + 1)^2 - 8 \cdot (NIR - Red)})/2$	Structure; Further minimize the soil background influence while increase the dynamic range of vegetation signal
Red-NIR	Transformed SAVI[20]	TSAVI	$a \cdot (NIR - a \cdot Red - b)/(a \cdot NIR + Red - a \cdot b)$	Structure; Minimize the soil background influence and work well for LAI and APAR estimations
Red-NIR	Adjusted TSAVI[182]	ATSAVI	$a \cdot (NIR - a \cdot Red - b)/[a \cdot NIR + Red - a \cdot b + 0.08 \cdot (1 + a^2)]$	Structure; Minimize the soil background influence and work well for LAI and APAR estimations
VIS-NIR	Atmospherically Resistant Vegetation Index[26]	ARVI	$(NIR - RB)/(NIR + RB)$, $RB = Red - \gamma \cdot (Blue - Red)$	Structure; Minimize the atmospheric effect and work better for vegetated surfaces than for soils, but need the blue band
VIS-NIR	Soil Adjusted and Atmospherically Resistant Vegetation Index[26]	SARVI	$(1 + L) \cdot (NIR - RB)/(NIR + RB + L)$, $RB = Red - \gamma \cdot (Blue - Red)$	Structure; Minimize both the soil and atmospheric effects, but need the blue band
VIS-NIR	Enhanced Vegetation Index[25]	EVI	$2.5 \cdot (NIR - Red)/(NIR + 6 \cdot Red - 7.5 \cdot Blue + 1)$	Structure; Minimize both the soil and atmospheric effects, while sensitive to the BRDF effect and need the blue band
Red-NIR	two-band EVI without the blue-band[27]	EVI2	$2.5 \cdot (NIR - Red)/(NIR + 2.4 \cdot Red + 1)$	Structure; Minimize the soil background influence and no need the blue band, while sensitive to the BRDF effect

Red-NIR	Near-Infrared Reflectance of vegetation[4]	NIRv	$NDVI \cdot NIR$	Structure; Minimize the soil background influence, while sensitive to the BRDF effect
VIS-NIR	Hyperspectral NIRv[153]	NIRvH	$NIR - Red - k(\lambda_{NIR} - \lambda_{Red})$	Structure; Further minimize the soil background influence, while sensitive to the BRDF effect
VIS-NIR	Fluorescence Correction Vegetation Index[29]	FCVI	$NIR - VIS$	Structure; Minimize the soil background influence, while sensitive to the BRDF effect
VIS-NIR	Kernel NDVI[31]	kNDVI	$\tanh(NDVI^2)$	Structure; Higher sensitivity to canopy structural parameters and GPP
VIS-NIR	Plant Phenology Index[28]	PPI	$-K \cdot \ln(\frac{M - DVI}{M - DVI_S})$	Structure; Linearly related to green LAI, less severely impacted by snow than NDVI and EVI, and work well for phenology at high latitudes, while need the soil DVI
VIS-NIR	Triangular Vegetation Index[183]	TVI	$0.5 \cdot [120 \cdot (R_{750} - R_{550}) - 200 \cdot (R_{670} - R_{550})]$	Structure; Biochemical: chlorophyll; Describe the radiation absorbed by the pigments
VIS-NIR	Modified Triangular Vegetation Index 1[59]	MTVI1	$1.2 \cdot [1.2 \cdot (R_{800} - R_{550}) - 2.5 \cdot (R_{670} - R_{550})]$	Structure; Insensitive to pigment changes, and better for LAI estimations than TVI
VIS-NIR	Modified Triangular Vegetation Index 2[59]	MTVI2	$1.5 \cdot [1.2 \cdot (R_{800} - R_{550}) - 2.5 \cdot (R_{670} - R_{550})]$ $/ \sqrt{(2 \cdot R_{800} + 1)^2 - (6 \cdot R_{800} - 5 \cdot \sqrt{R_{670}}) - 0.5}$	Structure; Minimize both the soil background and chlorophyll effects, while sensitive to LAI and thus a good LAI predictor

VIS-NIR	Modified Chlorophyll Absorption Ratio Index 1[59]	MCARI1	$1.2 \cdot [2.5 \cdot (R_{800} - R_{670}) - 1.3 \cdot (R_{800} - R_{550})]$	Structure; Less sensitive to chlorophyll variations than MCARI, while sensitive to LAI changes
VIS-NIR	Modified Chlorophyll Absorption Ratio Index 2[59]	MCARI2	$1.5 \cdot [2.5 \cdot (R_{800} - R_{670}) - 1.3 \cdot (R_{800} - R_{550})] / \sqrt{(2 \cdot R_{800} + 1)^2 - (6 \cdot R_{800} - 5 \cdot \sqrt{R_{670}}) - 0.5}$	Structure; Minimize both the soil background and chlorophyll effects, while sensitive to LAI and thus a good LAI predictor
VIS-NIR-MIR	MIR corrected NDVI[184]	NDVIc	$NDVI \cdot (1 - \frac{MIR - MIR_{min}}{MIR_{max} - MIR_{min}})$	Structure; Considered the canopy closure and understory contribution in LAI estimations by leaf water absorption of open canopies
VIS-NIR-SWIR	Reduced SR[23]	RSR	$SR \cdot (1 - \frac{SWIR - SWIR_{min}}{SWIR_{max} - SWIR_{min}})$	Structure; Increased the sensitivity and correlation to LAI than SR in boreal forests, while reduced the effect of background reflectance
Green-Red	Normalized Difference Greenness Index[185]	NDGI	$(Green - Red)/(Green + Red)$	Structure; Work well for identifying and mapping vegetation in inundated regions, no need the blue or NIR bands, and can work at PhenoCam imageries
Green-NIR	Green Chlorophyll Vegetation Index[186]	GCVI	$NIR/Green - 1$	Structure; Biochemical: chlorophyll; Depend on both LAI and chlorophyll concentration, and close relationship with LAI and green leaf biomass
Green-NIR	Green Difference Vegetation Index[187]	GDVI	$NIR - Green$	Biochemical: chlorophyll; Work well for predicting the late-season nitrogen requirement for corn

Green-NIR	Green Normalized Difference Vegetation Index[188]	GNDVI	$(NIR - Green)/(NIR + Green)$	Biochemical: chlorophyll; More sensitive to chlorophyll concentration than NDVI
Red edge-NIR	Red Edge Chlorophyll Index[33]	CIred-edge	$NIR/Re - 1$	Biochemical: chlorophyll; Linear relationship between the chlorophyll content in maize and soybean leaves with CIred-edge
Red edge-NIR	Red-edge NDVI[34]	NDVIre	$(NIR - RE)/(NIR + RE)$	Biochemical: chlorophyll; Directly proportional to chlorophyll and serve as indicators of leaf senescence
Red edge-NIR	MERIS Total Chlorophyll Index[35]	MTCI	$(R_{750} - R_{710})/((R_{710} - R_{680})$	Biochemical: chlorophyll; Correlate strongly with red-edge position and is sensitive to high values of chlorophyll content.
Red-Red edge	Chlorophyll Absorption Ratio Index[189,190]	CARI	$(R_{700} - R_{670}) - 0.2 \cdot (R_{700} - R_{550})$	Biochemical: chlorophyll; Minimize the effect of nonphotosynthetic materials in the FPAR estimations
Red-Red edge	Modified Chlorophyll Absorption in Reflectance Index[190]	MCARI	$[(R_{700} - R_{670}) - 0.2 \cdot (R_{700} - R_{550})] \cdot (R_{700}/R_{670})$	Biochemical: chlorophyll; Sensitive to leaf chlorophyll concentrations
Red-Red edge	Transformed Chlorophyll Absorption in Reflectance Index[191]	TCARI	$3 \cdot [(R_{700} - R_{670}) - 0.2 \cdot (R_{700} - R_{550}) \cdot (R_{700}/R_{670})]$	Biochemical: chlorophyll; Sensitive to chlorophyll over a wide range of variations, and is more sensitive to chlorophyll than MCARI

VIS-NIR	Pigment Specific Normalized Difference[192]	PSND	$(R_{800} - R_{675})/((R_{800} + R_{675})$ for Chl_a; $(R_{800} - R_{650})/((R_{800} + R_{650})$ for Chl_b; $(R_{800} - R_{500})/((R_{800} + R_{500})$ for Car;	Biochemical: chlorophyll, carotenoid; Strong relation with chlorophyll, while poor relation with carotenoid
VIS-NIR	Pigment Specific Simple Ratio[192]	PSSR	(R_{800}/R_{675}) for Chl_a; (R_{800}/R_{650}) for Chl_b; (R_{800}/R_{500}) for Car;	Biochemical: chlorophyll, carotenoid; Strong relation with chlorophyll, while poor relation with carotenoid
VIS-Red edge	Carotenoid Reflectance Index[193]	CRI	$1/R_{510} - 1/R_{550}$; $1/R_{510} - 1/R_{700}$	Biochemical: carotenoid; Remove the chlorophyll effect from the reflectance in the green edge range, and is sufficient to estimate the carotenoid content in plant leaves
VIS-Red edge	Plant Senescence Reflectance Index[38]	PSRI	$(R_{678} - R_{500})/R_{750}$	Biochemical: carotenoid, chlorophyll; Sensitive to the Car/Chl ratio, and can be used as a quantitative measure of leaf senescence/fruit ripening process
VIS	Normalized Pigments Chlorophyll Ratio Index[37]	NPCI	$(R_{680} - R_{430})/(R_{680} + R_{430})$	Biochemical: carotenoid, chlorophyll; Vary with the ratio of total pigments/Chl, indicative of plant phenology status
VIS-NIR	Structure Insensitive Pigment Index[36]	SIPI	$(R_{800} - R_{445})/((R_{800} - R_{680})$	Biochemical: carotenoid, chlorophyll a; Physiological; Minimize the confounding effects of the leaf surface and mesophyll structure, and provide the best semi-empirical estimation of the ratio of Car/Chla
Green-Red edge	Anthocyanin Reflectance Index[39]	ARI	$1/R_{550} - 1/R_{700}$	Biochemical: anthocyanin; An accurate estimation of anthocyanin accumulation

VIS-NIR	Modified Anthocyanin Reflectance Index[39,194]	MARI	$(1/R_{550} - 1/R_{700}) \cdot NIR$	Biochemical: anthocyanin; The best fit function with the Anthocyanin content, and yield accurate assessment
VIS	Red/Green Ratio Index[41]	RGRI	$Red/Green$	Biochemical: anthocyanin; Strongly related to pigment estimated by destructive sampling and spectrophotometric quantification
Green-NIR	Anthocyanin Content Index[40]	ACI	$\alpha_{Green}/\alpha_{NIR}$	Biochemical: anthocyanin; Linear relationship with total extractable anthocyanin content
Green-NIR	Modified Anthocyanin Content Index[195]	MACI	$NIR/Green$	Biochemical: anthocyanin, chlorophyll; Depends on three variables: chlorophyll, anthocyanin, and leaf thickness, and when the three vary independently, MACI becomes insensitive to anthocyanin.
NIR-SWIR	Normalized Difference Water Index[42]	NDWI	$\dfrac{NIR_{860} - SWIR_{1240}}{NIR_{860} + SWIR_{1240}}$	Biochemical: water content; Sensitive to vegetation water content changes, less sensitive to atmospheric effects than NDVI, while not completely remove the soil background reflectance effect as NDVI
NIR-SWIR	Land Surface Water Index[43,44]	LSWI	$\dfrac{R_{780\sim890} - R_{1580\sim1790}}{R_{780\sim890} + R_{1580\sim1790}}$	Biochemical: water content; A useful indicator for water content of evergreen needleleaf forest, useful for improving classification of cropland and forests, and improve the GPP estimations in the VPM model

NIR-SWIR	Normalized Difference Infrared Index[45]	NDII	$\dfrac{R_{850} - R_{1650}}{R_{850} + R_{1650}}$	Biochemical: water content; Related to canopy water content, linearly related to Equivalent Water Thickness (EWT) for corn, soybean and woodland
NIR-SWIR	Water Index[196]	WI	R_{900}/R_{970}	Biochemical: water content; Correlate with plant water concentration, and useful in evaluation of wild fire risk and drought
SWIR	Normalized Difference Lignin Index[47]	NDLI	$[\log(1/R_{1754}) - \log(1/R_{1680})]/[\log(1/R_{1754}) + \log(1/R_{1680})]$	Biochemical: lignin; Significantly correlate to foliar lignin concentration in green canopies, while unable to assess foliar or bulk canopy lignin in senescing vegetation
SWIR	Cellulose Absorption Index[197]	CAI	$100 \cdot [0.5 \cdot (R_{2019} + R_{2206}) - R_{2109}]$	Biochemical: cellulose; Positive for all crop residues, while all soils have negative values, and thus can discriminate crop residues from soil under dry and moist conditions
SWIR	Lignin Cellulose Absorption Index[198]	LCA	$100 \cdot [(R_{2185\sim2225} - R_{2145\sim2185}) + (R_{2185\sim2225} - R_{2295\sim2365})]$	Biochemical: lignin, cellulose; Linearly relate to crop residue cover with the R^2 higher than eight VIs in the evaluation
SWIR	Normalized Difference Nitrogen Index[47]	NDNI	$[\log(1/R_{1510}) - \log(1/R_{1680})]/[\log(1/R_{1510}) + \log(1/R_{1680})]$	Biochemical: nitrogen; Significantly correlate to foliar nitrogen concentration in green canopies, while unable to assess foliar or bulk canopy nitrogen in senescing vegetation

VIS	Photochemical Reflectance Index[49]	PRI	$(R_{531} - R_{570})/((R_{531} - R_{570})$	Physiological; Well track the diurnal changes of photosynthetic activity, but need to reduce complications associated with diurnal sun angle changes
VIS	Chlorophyll Carotenoid Index[5]	CCI	$\dfrac{Band_{11} - Band_1}{Band_{11} + Band_1}$	Physiological; Biochemical; Well track the seasonality of daily GPP and phenology for evergreen conifers at multiple spatial scales, and can be acquired at the global scale with MODIS data compared to PRI
VIS	Green Chromatic Coordinate[50,199]	GCC	$Green/(Red + Green + Blue)$	Physiological; Structure; Biochemical; Sensitive to changes in both carotenoid and chlorophyll, correlate well with GPP seasonality but less than CCI and PRI, and can be easily acquired using RGB imagery
Red edge	Red-edge Vegetation Stress Index[52]	RVSI	$(R_{714} + R_{752})/2 - R_{733}$	Physiological; Useful in the detection of stressed leaves in grapevine leafroll disease
VIS	Enhanced Bloom Index[200]	EBI	$\dfrac{Red + Green + Blue}{\frac{Green}{Blue} \cdot (Red - Blue + \varepsilon)}$	Physiological; Structure; Biochemical; Reduce the soil and green vegetation background noise, and can capture the flower information using RGB imagery from ground to satellites

1314

Box 1: **Physical clarification of a few VIs and SIF on their linkages and differences**

DVI is defined as the difference between the NIR and Red bands[19]:

$$DVI = NIR - Red \quad (1)$$

Here we demonstrate the linkage between NIRv and other VIs such as DVI, EVI and EVI2, by using DVI as the bridge among them. By definition, NIRv can be derived as the product of DVI and NIR/(NIR+Red)[4].

$$NIRv = NDVI \cdot NIR = \frac{NIR-Red}{NIR+Red} \cdot NIR = DVI \cdot \frac{NIR}{NIR+Red} \sim DVI \quad (2)$$

$$EVI = 2.5 \cdot \frac{NIR-Red}{NIR+6 \cdot Red-7.5 \cdot Blue+1} = DVI \cdot \frac{2.5}{NIR+6 \cdot Red-7.5 \cdot Blue+1} \sim DVI \quad (3)$$

$$EVI2 = 2.5 \cdot \frac{NIR-Red}{NIR+2.4 \cdot Red+1} = DVI \cdot \frac{2.5}{NIR+2.4 \cdot Red+1} \sim DVI \quad (4)$$

Below we show the linkage and difference between NDVI, SR and SAVI. Note when L in SAVI is 0, SAVI is equal to NDVI.

$$NDVI = \frac{NIR-Red}{NIR+Red} = \frac{SR-1}{SR+1} = 1 - \frac{2}{SR+1} \quad (5)$$

$$SR = NIR/Red \quad (6)$$

$$SAVI = (1+L) \cdot \frac{NIR-Red}{NIR+Red+L} \quad (7)$$

Based on spectral invariants theory, NIRv and SIF/PAR can be modelled in similar formula[81]:

$$NIRv = FPAR \cdot \omega \cdot f_{esc} \quad (8)$$
$$SIF/PAR = FPAR \cdot \Phi_F \cdot f_{esc} \quad (9)$$

where *fesc* is the photon escape probability from the canopy, ω is the leaf single scattering albedo in the NIR band, which is close to 1 in the NIR band, and Φ_F is the fluorescence yield. Rearranging Eqs. 8 and 9 gives

$$NIRv:(SIF/PAR) = \omega:\Phi_F \quad (10)$$

Glossary

1316 **Glossary**

1317 AVHRR: Advanced Very High Resolution Radiometer

1318 CHIME: Copernicus Hyperspectral Imaging Mission for the Environment

1319 DESIS: DLR Earth Sensing Imaging Spectrometer

1320 DSCOVR: Deep Space Climate Observatory

1321 EnMap: Environmental Monitoring and Analysis Program

1322 EPIC: Earth Polychromatic Imaging Camera

1323 ETM+: Enhanced Thematic Mapper Plus

1324 FLEX: FLuorescence EXplorer

1325 GIMMS-3g: Global Inventory Modeling and Mapping Studies-3rd generation

1326 GOES: Geostationary Operational Environmental Satellite

1327 HiSUI: Hyper-spectral Imager SUIte

1328 LTDR4: Long Term Data Record version 4

1329 MAIAC: Multi-Angle Implementation of Atmospheric Correction

1330 MERIS: MEdium Resolution Imaging Spectrometer

1331 MODIS: MODerate resolution Imaging Spectroradiometer

1332 MSG: Meteosat Second Generation

1333 PACE: Plankton, Aerosol, Cloud, ocean Ecosystem

1334 PRISMA: PRecursore IperSpettrale della Missione Applicativa

1335 SBG: Surface Biology and Geology

1336 SEVIRI: Spinning Enhanced Visible and Infrared Imager

1337 SPOT-VGT: Systeme Pour l'Observation de la Terre VEGETATION

1338 TEMPO: Tropospheric Emissions: Monitoring of Pollution

1339 VIIRS: Visible Infrared Imaging Radiometer Suite

1340 VIP3: Vegetation Index and Phenology version 3

Acknowledgements

Author contributions

1352 Y. Z., D. H., A. H., J. B., G. A. and M. C. wrote the synopsis and the initial draft of the manuscript.
1353 B. D., J. C., J. J., C. F., B. L., Y. R. and J. X. reviewed and edited the manuscript before
1354 submission. All authors made substantial contributions to the improvement of manuscript.

Competing interests

1356 The authors declare no competing interests.